HHS Public Access

Author manuscript

Mol Cell. Author manuscript; available in PMC 2024 October 19.

Published in final edited form as:

Mol Cell. 2023 October 19; 83(20): 3642–3658.e4. doi:10.1016/j.molcel.2023.09.003.

ATR Promotes Clearance of Damaged DNA and Damaged Cells by Rupturing Micronuclei

Yoon Ki Joo[1,2], **Elizabeth M. Black**[1,2], **Isabelle Trier**[1,2], **Wisse Haakma**[3], **Lee Zou**[3,4,5,6,7], **Lilian Kabeche**[1,2,6]

[1]Department of Molecular Biophysics and Biochemistry, Yale University, New Haven, CT 06511

[2]Yale Cancer Biology Institute, Yale University, New Haven, CT 06516

[3]Massachusetts General Hospital Cancer Center, Harvard Medical School, Charlestown, MA 02129, USA

[4]Department of Pathology, Massachusetts General Hospital, Harvard Medical School, Boston, MA 02114, USA

[5]Department of Pharmacology and Cancer Biology, Duke University School of Medicine, Durham, NC 27708, USA

Summary

The human ATR kinase functions in the nucleus to protect genomic integrity. Micronuclei (MN) arise from genomic and chromosomal instability and cause aneuploidy and chromothripsis, but how MN are removed is poorly understood. Here, we show that ATR is active in MN and promotes their rupture in S phase by phosphorylating Lamin A/C at Ser395, which primes Ser392 for CDK1 phosphorylation and destabilizes the MN envelope. In cells harboring MN, ATR or CDK1 inhibition reduces MN rupture. Consequently, ATR inhibitor (ATRi) diminishes activation of the cytoplasmic DNA sensor cGAS and compromises cGAS-dependent autophagosome accumulation in MN and clearance of micronuclear DNA. Furthermore, ATRi reduces cGAS-mediated senescence and killing of MN-bearing cancer cells by natural killer cells. Thus, in addition to the canonical ATR signaling pathway, an ATR-CDK1-Lamin A/C axis promotes MN rupture to clear damaged DNA and cells, protecting the genome in cell populations through unexpected cell-autonomous and nonautonomous mechanisms.

eTOC blurb

[6]Corresponding authors: lilian.kabeche@yale.edu; lee.zou@duke.edu.
[7]·Lead contact

Author Contributions: L.K., Y.J. and L.Z. designed the study. L.K., Y.J., E.B, I.T and W.H. performed the experiments and analyses. L.Z. and L.K. supervised the experiments and analyses. Y.J., L.K. and L.Z. prepared the manuscript with contributions from all authors.

Declaration of Interests: All authors do not have competing interests. L.Z. is a member of the advisory board of Molecular Cell.

Joo et al. uncovers a surprising role for ATR in promoting rupture of micronuclei (MN). ATR phosphorylates Lamin A/C at S395 and primes S392 for CDK1 phosphorylation, destabilizing the MN envelope. ATR-driven MN rupture activates cGAS and downstream cell autonomous and non-autonomous processes, protecting genomic integrity in cell populations.

Graphical Abstract

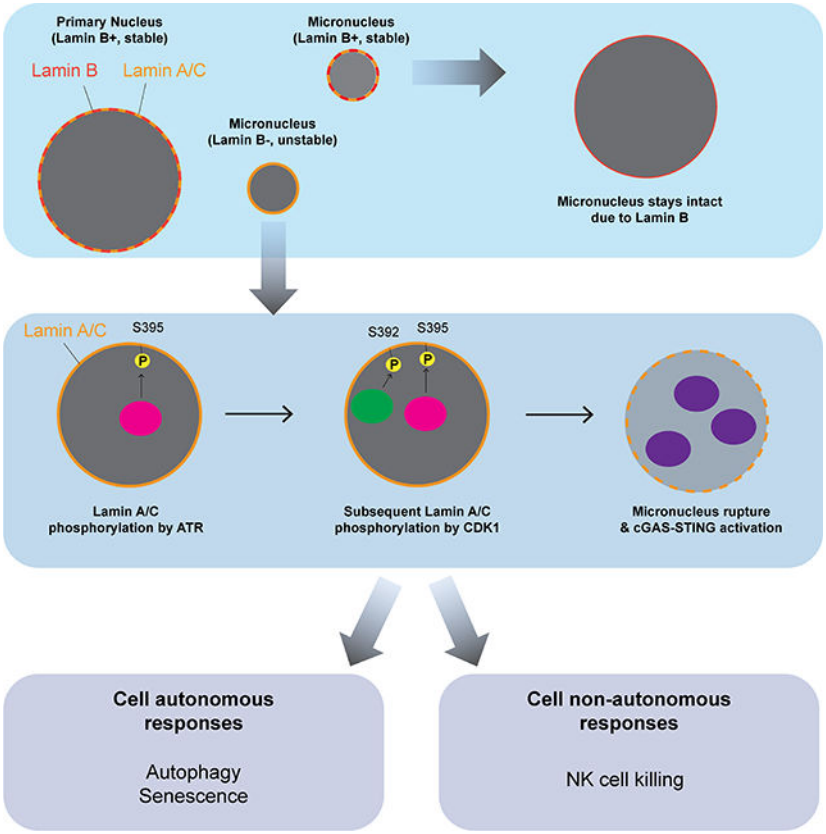

Introduction

The ataxia telangiectasia-mutated and Rad3-related (ATR) kinase is a master regulator of cellular responses to DNA damage and DNA replication stress in human cells.[1] In response to DNA damage or replication stress, the ATR-ATRIP kinase complex is activated following recruitment to DNA damage sites or stalled replication forks.[2] During S phase, ATR and its effector kinase Chk1 protect the replicating genome by phosphorylating numerous proteins involved in DNA replication, DNA repair, and cell-cycle control.[3] ATR stabilizes DNA replication forks and suppresses replication origin firing, partially through CDK2 inhibition by ATR and Chk1-mediated CDC25A degradation.[4] At the S-G2 transition, ATR restricts the activity of CDK1 to prevent premature entry into G2.[5] ATR also enables a G2-M checkpoint in the presence of DNA damage or incomplete DNA replication.[6] If the G2-M checkpoint is lost, cells enter mitosis with DNA damage, giving rise to mitotic defects and chromosomal instability (CIN).[7] During mitosis, ATR promotes accurate chromosome segregation by facilitating Aurora B activation.[8] Loss of ATR activity therefore results in

increased replication stress and genome instability in S phase, as well as elevated CIN in mitosis.[9–11] Thus, ATR acts on genomic DNA and protects the genome through discrete mechanisms. ATR is also suggested to sense mechanical stress at the nuclear envelope.[12] These functions of ATR are believed to be cell-autonomous and confined within the nucleus during the interphase. Whether ATR can function outside of the nucleus or exert cell-nonautonomous effects is not known.

Micronuclei (MN) arise from missegregation of whole chromosomes or chromosome fragments during mitosis. MN formation can be stimulated by agents or genetic perturbations that increase either chromosome missegregation in mitosis or induce DNA damage or replication stress prior to mitosis. The entrapment of chromosomes in MN leads to aneuploidy,[13] and are associated with prolonged transcription repression and DNA damage.[14,15] Furthermore, MN can result in genomic instability through chromothripsis, a process of severe chromosomal rearrangement in confined genomic regions.[16] The lamina and nuclear pore complexes of the nuclear envelope (NE) of MN are deficient compared to that of primary nuclei (PN).[17,18] Because of this deficiency, MN are susceptible to rupture, particularly in S phase.[17,18] The rupture of MN triggers the cGAS-STING pathway, thereby activating the type-I interferon (IFN) response and innate immunity.[19,20] Activation of the cGAS-STING pathway can also induce autophagy and senescence.[21,22] Furthermore, the cGAS-STING pathway is implicated in anti-tumor immunity, which involves both tumor cells and immune cells in the tumor microenvironments.[23] Thus, MN are not only a source of genomic instability and aneuploidy, but also a possible trigger of multiple responses in or around damaged cells.

Given the negative impacts of MN on genomic and chromosomal stability, the removal of MN or MN-bearing cells could be important for maintaining genomic integrity in cell populations. How MN are removed is not well understood. Live-cell imaging analysis shows that some MN ruptured in S phase can be reincorporated into PN after mitosis.[16] Indeed, the chromosome fragments entrapped in MN can reintegrate into the genome after undergoing chromothripsis, leaving ‘chromothripsis scars’.[16] Reintegration of MN chromosomes to the genome also results in heritable transcription loss and DNA damage.[14,15] Notably, chromothripsis is triggered by MN rupture, raising the possibility that the MN with compromised envelopes are particularly threatening to the genome and cells may actively remove these MN to protect genomic integrity. Upon MN rupture, the endoplasmic reticulum-associated nuclease TREX1 enters MN, degrades micronuclear DNA, and limits cGAS activation.[24] Furthermore, the autophagy proteins LC3 and p62 localize to the MN with damaged envelopes, which is associated with the degradation of micronuclear DNA.[25] Interestingly, the autophagy-mediated clearance of MN is dependent on cGAS, which is activated in ruptured MN.[26] Together, these results suggest that MN rupture may play an important role in the removal of MN. Nonetheless, whether MN rupture is a passive or regulated event remains unclear. Furthermore, why MN are particularly prone to rupture in S phase has not been addressed.

In this study, we unexpectedly find that ATR promotes rupture of Lamin B1-deficient (Lamin B1^{-}) MN. Mechanistically, ATR phosphorylates Lamin A/C at Ser395, priming Ser392 for CDK1 phosphorylation, thereby destabilizing Lamin A/C polymers in MN

envelope and increasing rupture. Notably, ATR inhibition reduces MN rupture and subsequent cGAS activation in MN. Consequently, several cGAS-regulated cellular processes, including autophagy, senescence, and the IFN response, are compromised, leading to defective removal of micronuclear DNA and reduced killing of MN-bearing cells by natural killer (NK) cells. These results reveal that ATR not only suppresses the instability of chromosomal DNA, but also promotes the clearance of damaged DNA and damaged cells through both cell-autonomous and nonautonomous mechanisms, substantially extending our appreciation of the functions of ATR in genome protection.

Results

ATR inhibition reduces MN rupture

To investigate how MN rupture, we stimulated MN formation by increasing replication stress with replication inhibitor aphidicolin (APH) or inhibitors of the ATR kinase (ATRi; VE-821 or AZ20). Alternatively, we induced whole chromosome missegregation with an inhibitor of the mitotic checkpoint kinase MPS1 (MPS1i, reversine). Treatment of the chromosomally unstable cancer cell line U2OS with APH, ATRi, or MPS1i for 24 hours increased the fraction of cells containing MN (Fig. 1A).[27] ATRi also increased the fraction of cells containing MN in chromosomally unstable cancer cell lines MDA-MB-231 and HeLa (Fig. S1A–B).[28,29] The combination of APH with ATRi further increased the fraction of MN-bearing U2OS cells, but co-treatment with MPS1i and ATRi did not increase MN further compared to MPS1i alone, possibly because the effects of MPS1i were dominant (Fig. 1A). In chromosomally stable DLD-1 cells and BJ fibroblasts,[30,31] MPS1i also increased the fraction of cells containing MN (Fig. S1C–D). Co-treatment with MPS1i and ATRi further increased MN in DLD-1 cells, but not in BJ cells where MPS1i alone induced MN robustly (Fig. S1C–D). Thus, ATRi generally increases MN formation in chromosomally stable or unstable cells.

To measure the rate of MN rupture, we quantified the fraction of MN positive for cGAS, which localizes into MN upon rupture.[19,20] Consistent with previous studies, approximately 25–45% of MN were $cGAS^+$ in U2OS, MDA-MB-231, and HeLa cells (Fig. 1B–D, S1E). Coimmunostaining of cGAS and ACA, a centromere marker, showed that cGAS was present in both ACA^+ and ACA^- MN (Fig. S1F), indicating that MN undergo rupture regardless of whether they contain whole chromosomes or chromosome fragments. Treatment of U2OS cells with APH or MPS1i increased the fraction of $cGAS^+$ MN (Fig. 1B), possibly caused by the poor association of non-core NE proteins with missegregated chromosomes.[17] MPS1i also increased the fraction of $cGAS^+$ MN in DLD-1 and BJ cells (Fig. 1E–F). Surprisingly, ATR inhibition in U2OS reduced the fraction of $cGAS^+$ MN in both the absence and presence of APH or MPS1i (Fig. 1B). ATRi also reduced the fraction of $cGAS^+$ MN in MDA-MB-231 and HeLa cells, as well as in MPS1i-treated DLD-1 and BJ cells (Fig. 1C–F). To induce MN without inhibitors, a GFP-tagged dominant negative mutant of the microtubule-depolymerizing Kinesin-13 (dnMCAK), which increases chromosome missegregation,[32,33] was transiently expressed in U2OS cells. dnMCAK increased the fraction of cells containing MN, whereas wild-type MCAK did not (Fig. S1G, left panel).

Furthermore, ATRi reduced the cGAS$^+$ MN in cells overexpressing dnMCAK (Fig. S1G, right panel). These results reveal an unexpected inhibitory effect of ATRi on MN rupture.

ATR promotes MN rupture independently of MN formation

To investigate how ATRi affects MN rupture, we tested whether the effects of ATRi on MN formation and rupture were separable. We treated U2OS, MDA-MB-231, and HeLa cells with ATRi for 1 hour, a timeframe too short for ATRi to cause chromosome mis-segregation.[5,8,11,34] Indeed, the fraction of cells carrying MN was not changed significantly by ATRi in 1 hour (Fig. S2A–C). However, the fraction of cGAS$^+$ ruptured MN was reduced by ATRi (Fig. S2D–F). Inhibitors of Chk1 (Chk1i) and ATM (ATMi) did not increase MN-bearing cells or reduce cGAS$^+$ MN in U2OS and MDA-MB-231 cells in 1 hour (Fig. S2A–B, S2D–E), suggesting that ATR functions independently of Chk1 and ATM to promote MN rupture. To test whether ATRi affects MN rupture under oncogene-induced replication stress, we analyzed U2OS cells overexpressing Cyclin E.[35] Induction of Cyclin E increased the fraction of cGAS$^+$ MN without altering the level of MN-bearing cells (Fig. S2G–H). Treatment with ATRi for 1 hour did not affect the level of Cyclin E-overexpressing cells that contained MN but reduced the fraction of cGAS$^+$ MN (Fig. S2I). Thus, ATRi rapidly reduces MN rupture without altering MN formation, suggesting that ATR has a rather direct role in promoting MN rupture.

Next, we used YFP-tagged nuclear localization signal (NLS) to monitor the rupture of both MN and primary nuclei (PN). As previously reported, NLS-YFP was only detected in cGAS$^-$ MN but not in cGAS$^+$ MN (Fig. S2J–K), confirming that NLS-YFP was lost from MN upon rupture.[19] Consistent with the decrease in cGAS$^+$ MN, ATRi treatment for 1 hour increased the fraction of NLS-YFP$^+$ MN (Fig. 1G), which was nearly 100% cGAS$^-$ (Fig. S2J). In marked contrast to MN, all the PN analyzed remained NLS-YFP$^+$ and showed no sign of rupture (Fig. 1G). These results suggest that ATRi specifically affects the rupture of MN but not PN.

To analyze the effects of ATRi on the kinetics of MN rupture, we used live-cell imaging to follow NLS-RFP-expressing U2OS cells after they were synchronously released from a nocodazole block in mitosis into media with or without ATRi (Fig. 1H–I). MN were readily detected 3.5 hours after nocodazole release as cells entered G1, and ATRi did not alter the abundance of MN (Fig. S2K). In the absence of ATRi, the fraction of NLS-RFP$^+$ intact MN rapidly declined over time, resulting in a >40% reduction after 10 hours (Fig. 1H–I). In the presence of ATRi, the fraction of intact MN declined more slowly, showing only a <20% reduction in 10 hours (Fig. 1H–I). In contrast to MN rupture, the rupture of PN tends to be transient, leading to reduced NLS-RFP signals in PN.[36] During the 24-hour time course, ATRi did not induce any rupture events or reduce RFP signals in PN (Fig. S2L–M). Thus, ATR specifically accelerates MN rupture after their formation.

ATR is active in the MN undergoing replication and promotes rupture in S phase

MN are known to undergo defective and asynchronous DNA replication,[37] prompting us to ask whether ATR is active in the MN undergoing replication.[11] We used EdU to label S-phase cells, NLS-YFP to identify intact PN and MN, and immunostained phosphorylated

ATR (p-ATR, T1989) or RPA32 (p-RPA32, S33), two markers of ATR activity (Fig. S3A–B). As expected, all S-phase PN were positive for EdU, p-ATR, and p-RPA32 (Fig. 2A, S3C), consistent with the role of ATR during DNA replication. In S-phase cells displaying EdU^+ PN, most but not all MN were EdU^+ (Fig. S3D–E), showing that PN and MN don't always undergo replication synchronously. Most of the MN in S-phase cells displayed p-ATR and p-RPA32 signals, which were reduced by ATRi (Fig. 2B). Notably, ~100% of the EdU^+ MN were also positive for p-ATR and p-RPA32 (Fig. 2C, S3D). When EdU^+ and EdU^- MN in S-phase cells were compared, EdU^+ MN displayed more p-ATR and p-RPA32 (Fig. S3F–G). Thus, the activation of ATR in MN is associated with the DNA replication in MN but not PN. When the p-ATR and p-RPA32 signals in intact and ruptured MN were compared, intact MN displayed stronger signals (Fig. S3F–G). γH2AX, a marker of DNA damage, did not associate with p-ATR in MN (Fig. S3H). Furthermore, ATRi did not affect γH2AX in intact MN (Fig. S3I). Hence, ATR is likely activated by replication stress but not DNA damage in intact MN.

To test whether ATR promotes MN rupture during S phase, we compared the effects of ATRi on MN in G1, S, and G2 cells. Cells were synchronized at G2/M with CDK1 inhibitor (CDK1i; RO-3306), released into mitosis in MPS1i to induce MN, and then allowed to progress through the cell cycle in the presence or absence of ATRi (Fig. 2D). During the following cell cycle, cells were pulse-labeled with EdU and stained with DAPI to distinguish G1, S, and G2 phases (Fig. 2D). In the absence of ATRi, the fraction of cells containing intact MN was high in G1 and declined in S and G2 (Fig. 2D). ATRi treatment did not alter the levels of MN and intact MN in G1 but reduced the decline of intact MN in S and G2 (Fig. 2D), suggesting that ATRi inhibited MN rupture in S phase. After NLS-RFP-expressing U2OS cells were synchronously released from a nocodazole block in mitosis, the fraction of intact MN started to decline in 5 hours as cells entered S phase (Fig. 2E). Blocking the G1/S transition with CDK2 inhibitor (CDK2i) substantially reduced the decline of intact MN, resembling the effects of ATRi (Fig. 2E). Co-treatment with ATRi and CDK2i reduced the decline of intact MN similarly as ATRi or CDK2i alone (Fig. 2E), supporting the idea that the effects of ATRi are dependent on S phase entry. Thus, ATR is active in the MN undergoing replication and promotes their rupture in S phase.

ATR acts with CDK1 to rupture Lamin B1-deficient MN

The susceptibility of MN to rupture is linked to Lamin B1 insufficiency in the NE of MN.[18] In contrast to PN, which were 100% Lamin $B1^+$, only ~50% of MN were Lamin $B1^+$ (Fig. S3J). In the Lamin $B1^-$ subpopulation of MN, ATRi decreased the fraction of NLS-YFP^- ruptured MN (Fig. 2F, S3K). In contrast, in the Lamin $B1^+$ subpopulation of MN, ATRi did not alter the fraction of ruptured MN (Fig. 2G, S3K), suggesting that the effects of ATRi on MN rupture are specific to Lamin $B1^-$ MN. When GFP-tagged Lamin B1 was transiently expressed in cells, ATRi did not affect the rupture of the GFP^+ MN (Fig. 2H). This stabilizing effect of exogenous Lamin B1 in MN is consistent with a previous study using Lamin B2 overexpression.[18] These results suggest that ATR preferentially promotes the rupture of Lamin $B1^-$ MN.

The phosphorylation of Lamin A/C by CDK1 promotes the disassembly of Lamin filaments.[38,39] CDK1 phosphorylates Lamin A/C at S22 and S392, destabilizing Lamin head-to-tail polymers.[40] The phosphorylation of Lamin A/C by CDK1 also reduces the localization of Lamin A/C to the NE of PN.[5,41] While CDK1 is best known for its role in the entry into mitosis, it also functions in S phase.[5,41] Therefore, we asked whether ATR affects the phosphorylation of Lamin A/C by CDK1 in S phase, which may destabilize Lamin filaments, particularly in Lamin B1^{-} MN. To test this hypothesis, we first checked whether CDK1 is present in MN in S-phase cells. Consistent with previous studies, CDK1 was predominantly cytoplasmic in S phase (Fig. 3A).[42] Notably, however, the majority of MN had equal or slightly higher levels of CDK1 compared to the cytoplasm of the same cells (Fig. 3A–B). Furthermore, MN generally had more CDK1 than PN in the same cells (Fig. 3A, 3C). In contrast, CDK1 p-Y15, an inhibited form of CDK1, was slightly less abundant in MN than in PN (Fig. 3D). Thus, CDK1 is present and likely active in a large fraction of MN in S phase.

To analyze the effects of CDK1 on MN rupture, we let MPS1i-treated mitotic cells synchronously progress to G1, S, and G2 in the presence or absence of CDK1i (Fig. 3E). Like ATRi, CDK1i did not affect intact MN in G1 but reduced their decline in S and G2. Moreover, co-treatment with CDK1i and ATRi reduced MN rupture similarly as CDK1i alone, suggesting that ATR and CDK1 affect MN rupture through the same mechanism. Consistently, co-treatment of asynchronous U2OS cells with ATRi and CDK1i decreased cGAS^{+} ruptured MN similarly as CDK1i or ATRi alone (Fig. 3F). In contrast to CDK1i, Wee1 inhibitor (Wee1i), which increases CDK1 activity, increased the fraction of cGAS^{+} MN (Fig. 3G). In NLS-RFP-expressing U2OS cells synchronously released from a nocodazole block, CDK1i substantially reduced the decline of intact MN over time (Fig. 3H). The effects of CDK1i and CDK2i on MN rupture were similar (Fig. 3H), suggesting both S phase entry and the CDK1 activity in MN are needed for efficient rupture. Co-treatment with CDK1i and CDK2i reduced MN rupture similarly to CDK2i alone (Fig. 3H), indicating that CDK1i cannot affect MN rupture if S phase entry is blocked by CDK2i. These results suggest that ATR and CDK1 function together to promote MN rupture in S phase.

ATR primes Lamin A/C for CDK1 phosphorylation

To test whether the Lamin A/C in MN are phosphorylated by CDK1 in S phase, we pulse-labeled S-phase cells with EdU and analyzed Lamin A/C p-S22 or p-S392 by immunostaining (Fig. 4A). Lamin A/C p-S22 was not detected in MN, whereas >60% of MN were positive for p-S392 (Fig. 4B). Treatment of cells with CDK1i for 1 hour significantly reduced the p-S392 in MN of S-phase cells (Fig. 4C–D), confirming the dependency of p-S392 on CDK1 activity. CDK1i also increased the periphery-to-internal ratio of GFP-Lamin A fluorescence in MN (Fig. 4E–F), providing evidence that the NE of MN is stabilized by CDK1i. Like CDK1i, ATRi also reduced Lamin A/C p-S392 and increased the periphery-to-internal ratio of GFP-Lamin A in MN of S-phase cells (Fig. 4C–F). These results suggest that ATR and CDK1 function together to promote the phosphorylation of Lamin A/C at S392.

To investigate how ATR and CDK1 contribute to Lamin A/C phosphorylation, we immunoprecipitated Lamin A/C from U2OS cells (Fig. 4G). The Lamin A/C from cells treated with CDK1i or ATRi displayed a reduction in p-S392. CDK1i and ATRi also reduced the overall phosphorylation of Lamin A/C at CDK substrate sites (p-S/T-P). Interestingly, ATRi but not CDK1i reduced the phosphorylation of Lamin A/C at S/T-Q sites, a motif of ATR substrates. These results indicate that ATR directly phosphorylates Lamin A/C at one or more S/T-Q sites, which in turn primes S392 for CDK1 phosphorylation. Since most of the immunoprecipitated Lamin A/C was presumably from PN, ATR and CDK1 likely phosphorylate Lamin A/C in both PN and MN.[43] The selective destabilizing effects of Lamin A/C phosphorylation on MN may be attributed to the fact that a large fraction of MN is deficient for Lamin B1 and contains more CDK1 than PN (Fig. 3C, S3J).[17]

We next sought to identify the ATR substrate site(s) in Lamin A/C. Lamin A S395, which is phosphorylated in cells,[44] resides in an S/T-Q motif. Importantly, the fraction of MN positive for Lamin A p-S392 was reduced when the Lamin A^{S395A} mutant was expressed in cells (Fig. 4H–I), suggesting that S395 is required for the efficient phosphorylation of S392. In contrast, when wild-type Lamin A (Lamin A^{WT}), Lamin A^{S392A}, and Lamin A^{S392D} were expressed in cells and immunoprecipitated, they did not display marked differences in p-S/T-Q (Fig. 4J), suggesting that S392 is not critical for S395 phosphorylation. These results support the idea that ATR phosphorylates Lamin A/C at S395 to prime S392 for CDK1 phosphorylation (see Fig. 4L).

Lamin A phosphorylation at S392/S395 is required for efficient MN rupture

To understand the impact of Lamin A/C phosphorylation on MN rupture, we tested a panel of Lamin A phosphorylation site mutants in U2OS cells (Fig. S4A–B). In cells without exogenous Lamin A, MPS1i reduced the fraction of NLS-YFP^+ intact MN as shown above (Fig. S4C). The MPS1i-induced reduction in intact MN was reversed by ATRi (Fig. S4C), confirming the inhibitory effects of ATRi on MN rupture. When mCherry-tagged Lamin A^{WT} was overexpressed in cells, it did not change the fraction of intact MN (Fig. 4K) or the effects of MPS1i and ATRi on intact MN (Fig. S4C–D). Thus, unlike the overexpression of Lamin B1 (Fig. 2H) and B2,[18] Lamin A^{WT} overexpression does not alter MN rupture, which is consistent with the idea that Lamin B1 is the limiting factor affecting MN rupture.[18] However, overexpression of Lamin A^{S392A}, a mutant lacking the S392 phosphorylation site, increased the fraction of intact MN and overrode the effects of MPS1i and ATRi (Fig. 4K, S4E), suggesting that Lamin A^{S392A} stabilizes MN in a dominant manner. In contrast, overexpression of Lamin A^{S392D}, which carries a phospho-mimicking mutation at S392, reduced the fraction of intact MN regardless of the presence or absence of MPS1i and ATRi (Fig. 4K, S4F), showing that Lamin A^{S392D} destabilizes MN dominantly. These results support a model in which the phosphorylation of Lamin A/C S392 by CDK1 directly destabilizes MN.

Reminiscent to Lamin A^{S392A}, Lamin A^{S395A} also increased the fraction of intact MN and overrode the effects of MPS1i and ATRi (Fig. 4K, S4G), suggesting that MN are similarly stabilized by the loss of ATR phosphorylation at S395 or CDK1 phosphorylation at S392. In cells overexpressing Lamin A^{S395D}, the fraction of intact MN was reduced regardless

of the presence or absence of MPS1i and ATRi (Fig. 4K, S4H), recapitulating the effects of Lamin A^{S392D}. Furthermore, overexpression of the Lamin $A^{S392A, S395A}$ double mutant increased the fraction of intact MN similarly to Lamin A^{S392A} and Lamin A^{S395A} single mutants (Fig. 4K, S4I). In contrast, overexpression of the Lamin $A^{S392D, S395D}$ double mutant destabilized MN as Lamin A^{S392D} and Lamin A^{S395D} single mutants (Fig. 4K, S4J). Thus, the phosphorylation of Lamin A/C S395 by ATR and S392 by CDK1 function together to promote MN rupture (Fig. 4L).

ATR promotes MN-induced cGAS activation

MN rupture activates cGAS, triggering several cell-autonomous and nonautonomous responses (Fig. 5A).[45] To test whether ATR modulates the cGAS-STING pathway by promoting MN rupture, we treated MDA-MB-231 and HeLa cells, both proficient for the cGAS-STING pathway,[32,46] with MPS1i and ATRi.[45] MPS1i treatment increased p-STING and p-IRF3 in MDA-MB-231 cells and p-STING in HeLa cells (Fig. 5B, S5A), supporting the idea that MN rupture promotes cGAS activation. Co-treatment with MPS1i and ATRi reduced MPS1i-induced p-STING and p-IRF3 in MDA-MB-231 cells and p-STING in Hela cells (Fig. 5B, S5A), suggesting that ATRi compromises cGAS activation by reducing MN rupture. To test whether ATR modulates the function of the cGAS-STING pathway, we analyzed the expression of several IFN-stimulated genes (ISGs). In DLD-1 cells treated with MPS1i, the expression of *ISG56* and *APOBEC3G* was similarly reduced by either ATRi or cGAS knockdown (Fig. S5B–D), consistent with the inhibitory effect of ATRi on cGAS activation. These results support the role of ATR in promoting cGAS activation and expression of ISGs.

In addition to the Type I IFN response, cGAS also induces cellular senescence (Fig. 5A).[47] Consistent with the stimulatory effects of MPS1i on cGAS activation, MDA-MB-231 cells treated with MPS1i displayed an increase in β-galactosidase staining, a marker of senescence (Fig. S5E). The MPS1i-induced β-galactosidase staining was partially reversed by ATRi, confirming the inhibitory effect of ATRi on cGAS activation. Furthermore, *IL-6* expression, an alternative marker of senescence,[48] was reduced by either ATRi or cGAS knockdown in DLD-1 cells treated with MPS1i (Fig. S5F), suggesting a role for ATR in promoting cGAS-induced senescence. Thus, ATR indeed modulates cGAS activation by affecting MN rupture.

ATR promotes the clearance of micronuclear DNA

Rupture of MN not only activates cGAS but also exposes micronuclear DNA to cytosolic proteins, which may enable the clearance of micronuclear DNA.[22,25] To test this possibility, we first analyzed the effects of MPS1i and ATRi on lipidated LC3 (LC3-II), the active form of LC3 in autophagosomes (Fig. 5A). Treatment of MDA-MB-231 cells with MPS1i increased LC3-II, and this increase was partially reversed by ATRi (Fig. 5C), supporting the notion that MN rupture promotes cGAS-mediated autophagy and ATRi dampens this process. Cytosolic puncta of p62, a component of autophagosome, were observed in MDA-MB-231 and U2OS cells (Fig. 5D, S5H).[49] Of note, although U2OS cells express low levels of STING,[50] they can still carry out cGAS-mediated autophagy in MN.[51] In MDA-MB-231 cells, p62 was detected in ~20% of total MN, but 60% of the $cGAS^{+}$ ruptured

MN were p62$^+$ (Fig. 5E), suggesting that p62 is enriched in ruptured MN. Importantly, the knockdown of cGAS in MDA-MB-231 reduced the fractions of total MN and ruptured MN containing p62 (Fig. 5E, S5G), demonstrating that p62 is recruited to ruptured MN in a cGAS-dependent manner. Consistent with the possibility that MN rupture activates cGAS to recruit p62, MPS1i increased the fraction of p62$^+$ MN in MDA-MB-231 and U2OS cells, and this increase was reversed by ATRi (Fig. 5F, S5I). Neither MPS1i nor ATRi changed the fraction of cGAS$^+$ MN that were p62$^+$ (Fig. S5J), suggesting that these inhibitors affect MN rupture but not the subsequent localization of p62 to ruptured MN. Similar to p62, RFP-LC3 was also detected in ~30% of MN (Fig. 5G).[26] RFP-LC3 was only detected in NLS-YFP$^-$ruptured MN (Fig. S5K). In addition, MPS1i increased RFP-LC3$^+$ MN, and this increase was reversed by ATRi (Fig. 5G). Together, these results suggest that ATR promotes MN rupture to enable the cGAS-mediated accumulation of autophagosomes in MN.

To test whether autophagosomes contribute to the clearance of micronuclear DNA, we used DAPI staining to semi-quantitatively measure the levels of DNA in MN. The levels of micronuclear DNA were lower in the ruptured and p62$^+$ MN than in the MN that were either intact or ruptured but p62$^-$ (Fig. 5H), supporting the idea that autophagy clears micronuclear DNA in ruptured MN. The overall reduction of micronuclear DNA in ruptured MN was partially suppressed by cGAS knockdown (Fig. 5I). Upon MPS1i treatment, the levels of micronuclear DNA were further reduced in p62$^+$ MN (Fig. 5J), possibly because MPS1i accelerates MN rupture and gives autophagosomes more time to degrade micronuclear DNA. The MPS1i-induced reduction in micronuclear DNA in p62$^+$ MN was partially reversed by ATRi (Fig. 5J), lending further support to the role of ATR in promoting MN rupture and subsequent autophagy-mediated MN clearance.

In addition to autophagy, the TREX1 nuclease is also implicated in the clearance of micronuclear DNA.[24] Similar to p62, TREX1 was detected in ~20% MN and ~60% ruptured MN (Fig. S5L), consistent with the accumulation of TREX1 in ruptured MN. The fractions of MN and ruptured MN containing TREX1 were increased by MPS1i, and this increase was reversed by ATRi (Fig. S5L). Thus, ATR inhibition reduces the clearance of micronuclear DNA by suppressing MN rupture and limiting the accumulation of both autophagosomes and TREX1 in MN.

ATR promotes NK cell-mediated killing of MN-bearing cells

Chromosome missegregation triggers killing of aneuploid cells by NK cells,[52] and the cGAS-STING pathway activates the NK cell response *in vivo*.[53] To test whether ATR-mediated MN rupture induces NK cell-mediated killing, we treated MDA-MB-231 cells with DMSO, MPS1i, or MPS1i and ATRi for 24 hours, and then co-cultured them with NK-90 cells for 3 hours. The killing of MDA-MB-231 cells by NK cells was determined by imaging every 15 minutes (Fig. 6A–B). Consistent with the stimulatory effects of MPS1i on MN rupture and cGAS activation, MPS1i increased the NK cell killing of MDA-MB-231 cells during a 3-hour time course (Fig. 6B). Notably, the stimulation of NK cell-mediated killing by MPS1i was partially reversed by ATRi (Fig. 6B, S6), suggesting that ATR modulates the NK cell response through MN rupture.

To ascertain that ATRi affects NK cell-mediated killing through the cGAS pathway, we knocked down cGAS in MDA-MB-231 cells (Fig. 6C). Consistent with the time course above, the presence of NK cells allowed MPS1i to further reduce the survival of MDA-MB-231 cells in 24 hours (Fig. 6C, columns 1–2 and 4–5), indicating NK cell-mediated killing. ATRi partially reversed the effect of MPS1i in the presence of NK cells (Fig. 6C, columns 5–6). However, when cGAS was knocked down, neither MPS1i nor ATRi affected the survival of MDA-MB-231 cells in the presence of NK cells (Fig. 6C, columns 7–9). Thus, the MPS1i-induced and NK cell-mediated killing of MDA-MB-231 cells, which is dampened by ATRi, is dependent upon cGAS. Similar observations were made in DLD-1 cells (Fig. 6D). These results suggest that ATR promotes the removal of cells bearing ruptured MN by stimulating NK cell-mediated killing, which occurs in a cGAS-dependent and cell-nonautonomous manner (Fig. 6E).

Discussion

ATR is a well-known safeguard of the genome. The known functions of ATR in genome protection are largely dependent on the ability of ATR to sense ssDNA at sites of DNA damage, stalled replication forks, R-loops, and other stress-associated DNA structures.[8,54–59] Upon activation, ATR phosphorylates numerous substrates on DNA or chromatin.[3,60] Through Chk1, ATR also regulates proteins distal to itself.[4,61–63] ATR has also been shown to sense mechanical stress of the NE.[12,64] All of these functions of ATR are executed in the PN in a cell-autonomous manner. In this study, we find that ATR plays an unexpected role in MN rupture, providing evidence that ATR also functions outside of the PN. By promoting MN rupture and subsequent cGAS activation, ATR protects genomic integrity in cell populations through autophagy, senescence, and NK cell-mediated killing of MN-bearing cells (Fig. 6E). Because senescence and the IFN response influence the tumor microenvironment (TME),[65,66] ATR not only functions outside of the nucleus but also exerts its effects outside of the cells in which it is activated. These findings substantially extend our understanding of where and how ATR functions to protect the genome.

How ATR is activated in MN is still unclear. Because the p-ATR in MN is tightly associated with the replication in MN (Fig. 2C, S3F), the activation of ATR in MN is likely triggered by the replication stress in MN but not PN. Our results are consistent with the previous report that the replication in MN is inefficient and asynchronous,[37] suggesting that ATR is activated in MN when they undergo compromised replication. A recent study suggested that R-loops, which generate ssDNA and interfere with replication forks, accumulate in MN,[67] suggesting a possible cause of replication stress in MN. Notably, the γH2AX in MN does not associate with p-ATR and is not ATR-dependent, indicating that ATR is not activated by DSBs. Furthermore, intact MN display more p-ATR than ruptured MN (Fig. S3F), suggesting that ATR is activated in MN before rupture. Together, our results support a model in which ATR is activated by the replication stress in MN prior to MN rupture and chromosome pulverization.

Our results reveal an intricate relationship between ATR and CDK1. The ATR-Chk1 pathway restricts CDK1/2 activities, ensuring proper S phase and S-G2 and G-M transitions. The function of ATR in antagonizing CDK1/2 is important for preventing replication stress,

CIN, and MN formation.[9–11,63,68] However, once MN are formed, ATR is active in MN during S phase to promote MN rupture by priming Lamin A/C for CDK1 phosphorylation (Fig. 6E). Thus, the interplays between ATR and CDK1/2 are context-dependent. On one hand, ATR restricts CDK1/2 activities to limit replication stress and coordinate cell-cycle transitions. On the other hand, ATR facilitates CDK1 in MN and possibly PN to phosphorylate specific substrates like Lamin A/C, controlling NE stability in MN and PN. These mechanisms may enable ATR to exert opposite effects on different CDK substrates, coordinating different cellular events during the cell cycle.

While ATR promotes MN rupture and the activation of cGAS in MN, it is important to remember that ATR also suppresses MN formation. The overall effects of ATR on cGAS activation may be determined by the balance of MN formation and rupture. In cells with high levels of CIN, MN may accumulate robustly despite the presence of ATR, and ATRi may mainly affect MN rupture. In contrast, in cells under high replication stress, the stimulatory effect of ATRi on MN formation may outweigh the reduction in MN rupture. Of note, ATRi stimulates radiation-induced immune responses.[34,69] In this context, radiation generates DNA damage and ATRi abolishes the G2-M checkpoint, thereby increasing the formation of MN robustly.

It is worth noting that ATR only promotes the rupture of Lamin $B1^-$ MN (Fig. 6E). Lamin $B1^-$ MN are known to be more rupture-prone and threatening to genomic stability.[18] In Lamin $B1^-$ MN, the stability of Lamin A/C polymers may be particularly important for the integrity of NE. Our finding that ATR promotes the rupture of Lamin $B1^-$ MN by phosphorylating Lamin A/C suggests that MN rupture is not a completely passive event, but a regulated process. Although ATR may also phosphorylate Lamin A/C at S395 in PN, the NE of PN is likely more stable because of the presence of Lamin B1 and the low abundance of nuclear CDK1 in S phase. Thus, the phosphorylation of Lamin A/C S395 by ATR in MN may provide a unique mechanism to preferentially remove a vulnerable subpopulation of MN.

By modulating MN rupture, ATR influences several cGAS-mediated processes. We observe that the autophagosome component p62 accumulates in ruptured MN in a cGAS-dependent manner. This finding is consistent with a recent report that cGAS acts as a receptor for autophagy in MN to clear micronuclear DNA.[26] cGAS is highly enriched in ruptured MN and it interacts with autophagosome protein MAP1LC3B, providing a mechanism to recruit autophagosomes to MN.[19,20,26] We also observe that TREX1 accumulates in ruptured MN.[24] The accumulation of both p62 and TREX1 in MN is increased by MPS1i but reduced by ATRi, suggesting that ATR promotes MN rupture and the subsequent clearance of micronuclear DNA by both autophagy and TREX1 (Fig. 6E). The activation of cGAS in cancer cells influences the TME. A previous study showed that the cGAS-STING pathway is activated by cytosolic DNA and MN in MDA-MB-231 cells, enhancing the expression of inflammatory genes.[32] In vivo, NK cells are activated by IFN-β, which is produced in tumors in a STING-dependent manner.[53] In our coculture experiments using MDA-MB-231 or DLD-1 cancer cells and NK cells, ATR promotes MN rupture in cancer cells and allows them to produce IFNs and elicit a NK cell response, establishing ATR as a modulator of the TME.

It is tempting to speculate that ATR-mediated MN rupture functions as a barrier to protect the genome against aneuploidy and chromothripsis. ATR may function in the nucleus to prevent MN formation, and also in MN to promote MN removal. The combination of these ATR functions may orchestrate a "double barrier" to suppress the negative impacts of MN on the genome. Of note, MN rupture not only triggers MN removal but also chromothripsis.[16] The reintegration of micronuclear DNA to chromosomes may be rare when ruptured MN are efficiently removed by autophagy and cytosolic nucleases. In this scenario, the role of ATR in promoting MN rupture and removal would suppress aneuploidy and genomic instability. However, if ruptured MN are not efficiently removed, ATR could potentially enhance chromothripsis and cause genomic instability. In future studies, it is critical to assess the effects of ATR on aneuploidy and chromothripsis directly in various physiological and pathological contexts.

Limitations of the Study

ATR promotes the overall phosphorylation of Lamin A/C at S392 and S395, suggesting that Lamin A/C polymers are destabilized by ATR in both PN and MN. Although we did not observe any effect of ATRi on the rupture of PN during our experiments, it remains possible that prolonged ATRi treatment could affect PN integrity. Whether the effects of ATR on Lamin A/C in PN contribute to the regulation of PN envelope during the cell cycle or stress responses remains to be investigated.

STAR * METHODS

RESOURCE AVAILABILITY

Lead Contact—Further information and requests for reagents should be directed to lead contact Lee Zou (lee.zou@duke.edu).

Materials availability—All unique materials generated in this study are available upon request.

Data and code availability

- All data reported in this paper are available upon request. All imaging and Western blot date shown in this paper have been deposited to Mendeley Data. Accession number and DOI are listed in the Key Resource Table.
- This paper does not report original code.
- Any additional information required to reanalyze the data reported in this paper is available from the lead contact upon request.

EXPERIMENTAL MODEL AND STUDY PARTICIPANT DETAILS

Cell lines and culture medium—U2OS (ATCC, HTB-96), HeLa (ATCC, CCL-2) and MDA-MB-231 (ATCC, HTB-26) cells were cultured in Dulbecco's modified Eagle's medium (DMEM; Invitrogen) supplemented with 10% FBS (Invitrogen) and 1% penicillin/streptomycin.

YFP-NLS expressing U2OS cell lines were generated by retroviral transfection of pQC NLS- YFP IX plasmid (gift from Connie Cepko; Addgene 37341). NLS-YFP cells were transiently transfected with pmRFP LC3 (gift from Tamotsu Yoshimori, Addgene 21075) using lipofectamine 3000 (ThermoFisher).

NK 92 mi (ATCC, CRL-2408) cells were cultured using Alpha Minimum Essential Medium without ribonucleosides and deoxyribonucleosides (GIBCO), supplemented 0.2mM inositol (Sigma-Aldrich), 0.1mM 2-mercaptoethanol, 0.02mM folic acid (Sigma-Aldrich), 12% horse serum (Invitrogen) and 12.5% fetal bovine serum (Invitrogen).

METHOD DETAILS

siRNA transfection—siRNA transfections were conducted using 10nM RNAi and Lipofectamine RNAiMAX reagent (Invitrogen), and cells were analyzed 48 hours later.

Small molecule inhibitor treatment—For all experiments, the following concentrations of inhibitors were used: VE-821 (ATRi, 10μM), AZ20 (ATRi, 1μM), RO-3306 (CDK1i, 10μM), MK-8776 (CHK1i, 2μM), K03861 (CDK2i, 5μM), Reversine (MPS1i, 0.5μM), KU-55933 (ATMi, 10μM), Aphidicolin (APH, 0.3μM).

Construction of Lamin A plasmids—The Phusion High-Fidelity DNA Polymerase kit (New England Biolabs) was used to insert the pENTR sequence ahead of an existing GFP-tagged lamin A gene. The recombinant gene was then inserted into an pENTR vector using the pENTR/D-TOPO cloning kit (Invitrogen) the insertion was validated by restriction enzyme digestion. The QuikChange II Site-Directed Mutagenesis Kit (Agilent Technologies) was used to perform site directed mutagenesis of the codons S392 and S395 of the LMNA gene into alanine and aspartic acid, a loss of function and phosphomimetic mutation respectively. The primers that were used for the site-directed mutagenesis and pENTR insertion are noted below. The mutations were confirmed by the MGH DNA core facility via Sanger sequencing before the Gateway LR Clonase II Enzyme mix (Thermo Fisher) was used to transfer the mutated and WT GFP-lamin A genes into the pDest 3X HA vector. For construction of Lamin A constructs containing mCherry tag, the open reading frame of WT Lamin A was amplified using the Phusion High-Fidelity Polymerase kit (New England Biolabs) and inserted into pCDNA-mCherry vector to have an N-terminal mCherry tag. Lamin A-GFP constructs used for immunoprecipitation was a gift received from John Eriksson's lab from Åbo Akademi University.

Plasmid transfection—Plasmid transfections were conducted using 1~5μg of plasmid DNA with Lipofectamine 3000 reagent (Invitrogen). In experiments that required co-transfection of two or more constructs, 0.5~2.5μg of each of the required plasmid was transfected. The transfection rate was analyzed the following day using Cytation 5 (Biotek).

RNA extraction and RT-qPCR analysis—Cells were grown to ~80% confluency and were treated with either MPS1 inhibitor (Reversine) alone or ATR inhibitor (VE-821) with MPS1 inhibitor for 20 hours. After 20 hours, cells were harvested using 0.05% Trypsin (Gibco) and washed 3X with ice-cold PBS. Washed cells were then used to extract RNA using RNeasy Plus Mini Kit (Qiagen, #74134).

For RT-qPCR analysis, ~300ng of the extracted RNA were injected into each well of 96-well plate (Bio-Rad, #MLL9601) containing mixture of reverse transcriptase (Luna Universal One-Step RT-qPCR Kit, NEB #E3005S) and iTaq Universal SYBR Green Supermix (Bio-Rad, #1725121). RT-qPCR reaction was performed in one-step in the 96-well plate with C1000 Touch Thermocycler with CFX96 Real-Time System (Bio-Rad). Amplification was monitored by measuring SYBR signal, which was automated by CFX96 Real-Time System. Following reaction, Cq values from amplification curves were calculated and obtained using CFX Manager software.

For analysis, Cq values of housekeeping genes (GAPDH or Tubulin) were subtracted from Cq values of genes of interest to obtain ΔCq. ΔCq of untreated samples were subsequently subtracted from ΔCq values of inhibitor-treated samples to obtain ΔΔCq. ΔΔCq was then used as an exponent to calculate the fold change in expression.

Immunofluorescence microscopy—Cells were fixed with 3.5% paraformaldehyde for 15 minutes, incubated with ice-cold methanol for 10 minutes, washed with PBS + 0.5% Triton X-100 for 5 minutes, and washed with PBS + 3% Bovine serum albumin (BSA) for 10 minutes. Antibodies were diluted in PBS + 1% BSA, and cells on coverslips were incubated with antibodies for 12 hours at 4°C. Cells were then washed with PBS for 5 minutes. Secondary antibodies were diluted in PBS + 1% BSA, and cells on coverslips were incubated with secondary antibodies for 1hour at room temperature (~25°C). Images were acquired on a Nikon Eclipse 90i with a Retiga 200R camera and processed in Photoshop CS4 (Adobe). Representative un-deconvoluted single stack images are shown.

For quantitative assessments of micronuclei frequency, unsynchronized cells were untreated (CONT) or treated with various inhibitors for 1 hour or 24 hours, and stained with DAPI to mark DNA. Micronuclei were defined as discrete DNA aggregates separate from the primary nucleus in cells where interphase primary nuclear morphology was normal. Cells with an apoptotic appearance were excluded.

For assessments of micronuclei intact and ruptured micronuclei, unsynchronized cells were untreated (CONT) or treated with various inhibitors for 1 hour or 24 hours, and subsequently fixed and stained. For S phase analysis, cells were treated with 10μM EdU for 30 minutes before fixation. EdU was stained with using the Click-IT EdU Kit (ThermoFisher).

For quantitative analysis of cells stained with CDK1, the average intensity in the MN was measured as defined by DNA stain and the same size measurement was taken in the main nucleus or in the cytoplasm. Subsequently, the ratio of MN to main nucleus or MN to cytoplasm was determined.

For quantitative analysis of micronuclei rupture through the cell cycle, U2-OS cells were synchronized with CDK1i (10μM RO-3306) for 16 hours or with 100ng/ml Nocodazole for 12 hours, and washed with PBS twice and new media was added. Cells were subsequently released into MPS1i (0.5μM reversine) and fixed and stained at 6 hours after release (G1), 12 hours after release (S phase) and 18 hours after release (G2). Cells were incubated with 10μM EdU for 30 minutes before fixation. For subsequent cell cycle analysis, DAPI average

intensity was plotted against log(EdU) intensity, which yielded three distinct clusters of population. G1 cells were scored for low DAPI signal and the absence of EdU signal, G2 cells were scored for high DAPI signal and the absence of EdU signal, and S phase cells were scored for the presence of EdU signal regardless of DAPI intensity.

Live cell imaging—Approximately 5×10^4 U2OS cells ectopically expressing Nuclear Localization Sequence tagged with Red Fluorescent Protein (NLS-RFP) were plated onto 24-well glass bottom imaging plate (Cellvis) and incubated overnight at 37°C and 5% CO2. The same wells were treated with 100ng/ml of Nocodazole the next day for 16 hours to synchronize and arrest cells at mitosis. After 16 hours of mitotic arrest, the media containing Nocodazole was aspirated and was replaced by fresh media containing 1μM Reversine (MPS1 inhibitor) to release cells from mitotic arrest and induce chromosome mis-segregation events. After three hours from the release, cells were treated with either no inhibitors, 10μM VE-821 (ATR inhibitor), 10μM RO3306 (CDK1 inhibitor), or combination of these inhibitors with 1μM K03861 (CDK2 inhibitor) to induce S phase arrest. After inhibitor treatments, automated microscopy with reflection-based laser autofocus was performed on Cytation 5 microscope (Biotek) equipped with 20X dry objective for 24 hours, with 30 minutes/frame. The microscope was maintained at 37°C and 5% CO2 for the duration of the imaging process.

The mean intensity of primary nuclei (PN) NLS-RFP signal was measured using ImageJ. PN were selected using the circle tool selecting a circle that most closely matched and remained inside the cell. Cells were followed throughout the duration of the imaging session. RFP-intensity was plotted where the first timepoint was normalized to 1.

NK92 cell killing assay—For live-cell imaging analysis, MDA-MB-231 were plated onto 96 well glass bottom dishes and treated with mock control, MPS1i or MPS1i and ATRi for 24 hours. Inhibitors were washed out twice with warm PBS and cells were placed in NK92mi growth medium and co-cultured in the presence of NK92mi cells at a target:effector ratio of 1:100 for over 3 hours. Cells were imaged every 15 minutes using a Zeiss LSM 710 inverted confocal microscope. Cells were maintained at 37°C with 5% CO_2. Cells were counted using ImageJ.

For crystal violet assay to determine NK92 cell killing, MDA-MB-231 and DLD-1 were plated onto 96 well flat bottom dishes and incubated with cGASsi for 24 hours, as above. Media was washed out and cells were subsequently treated with inhibitors for another 24 hours. Inhibitors were then washout twice with warm PBS and cell were placed in NK92mi growth medium and co-cultured in the presence of NK92mi cells at a target:effector ratio of 1:100 for 5 hours. Cells were then washed twice with PBS to remove NK92mi cells and fixed with crystal violet stain for 10 minutes, rinsed 5 times with PBS and measured using absorbance at 570 on a Synergy HTX Multi-mode reader (BioTek).

Immunoprecipitation—Asynchronous cells were either untreated or treated for 1 hour with ATRi or CDK1i. Cells were collected via trypsinization. Cells were then washed twice with ice-cold 1X PBS, and lysed with lysis buffer containing 0.5% NP-40, protease inhibitors, 100μM Okadaic Acid (Tocris 1136). Antibody-coupled Protein G Dynalbeads ®

(ThermoFisher) were added to lysates and incubated for 16 hours with rocking at 4°C. Beads were washed 3 times with lysis buffer (without benzonase) at 4°C before elution at 95 °C in SDS sample buffer.

QUANTIFICATION AND STATISTICAL ANALYSIS

Immunofluorescence intensities, and live-cell imaging cell counts were measured using Fiji software and displayed using Graphpad PRSM software. Gels were imaged using GelDoc Go System (BioRad) and analyzed with Fiji software. NK cell killing assay using crystal violet staining was analyzed using Gen5 software (BioTek). Unpaired Student's t-tests when comparing two conditions, Anova with Tukey's Multiple Comparison Test when comparing three or more conditions used for statistical analysis as shown in figure legends.

Supplementary Material

Refer to Web version on PubMed Central for supplementary material.

Acknowledgment:

We thank Drs. N. Dyson and M. Cobbold for reagents, and members of the Zou and Dyson labs for discussions. L.Z. was the James & Patricia Poitras Endowed Chair in Cancer Research. This work is supported by NIH grants CA244865 and R35GM150648 to L.K., F31CA275096 to E.B., and CA197779 and CA218856 to L.Z. This work was also supported by the Pershing Square Sohn Cancer Research Alliance Award to L.K.

Inclusion and Diversity:

We support inclusive, diverse, and equitable conduct of research.

References

1. Saldivar JC, Cortez D, and Cimprich KA (2017). The essential kinase ATR: ensuring faithful duplication of a challenging genome. Nat Rev Mol Cell Biol 18, 622–636. 10.1038/nrm.2017.67. [PubMed: 28811666]
2. Marechal A, and Zou L (2013). DNA damage sensing by the ATM and ATR kinases. Cold Spring Harb Perspect Biol 5. 10.1101/cshperspect.a012716.
3. Matsuoka S, Ballif BA, Smogorzewska A, McDonald ER 3rd, Hurov KE, Luo J, Bakalarski CE, Zhao Z, Solimini N, Lerenthal Y, et al. (2007). ATM and ATR substrate analysis reveals extensive protein networks responsive to DNA damage. Science 316, 1160–1166. 10.1126/science.1140321. [PubMed: 17525332]
4. Mailand N, Falck J, Lukas C, Syljuasen RG, Welcker M, Bartek J, and Lukas J (2000). Rapid destruction of human Cdc25A in response to DNA damage. Science 288, 1425–1429. 10.1126/science.288.5470.1425. [PubMed: 10827953]
5. Saldivar JC, Hamperl S, Bocek MJ, Chung M, Bass TE, Cisneros-Soberanis F, Samejima K, Xie L, Paulson JR, Earnshaw WC, et al. (2018). An intrinsic S/G2 checkpoint enforced by ATR. Science 361, 806–810. 10.1126/science.aap9346. [PubMed: 30139873]
6. Liu Q, Guntuku S, Cui XS, Matsuoka S, Cortez D, Tamai K, Luo G, Carattini-Rivera S, DeMayo F, Bradley A, et al. (2000). Chk1 is an essential kinase that is regulated by Atr and required for the G(2)/M DNA damage checkpoint. Genes Dev 14, 1448–1459. [PubMed: 10859164]
7. Nghiem P, Park PK, Kim Y, Vaziri C, and Schreiber SL (2001). ATR inhibition selectively sensitizes G1 checkpoint-deficient cells to lethal premature chromatin condensation. Proc Natl Acad Sci U S A 98, 9092–9097. 10.1073/pnas.161281798. [PubMed: 11481475]

8. Kabeche L, Nguyen HD, Buisson R, and Zou L (2018). A mitosis-specific and R loop-driven ATR pathway promotes faithful chromosome segregation. Science 359, 108–114. 10.1126/science.aan6490. [PubMed: 29170278]

9. Brown EJ, and Baltimore D (2003). Essential and dispensable roles of ATR in cell cycle arrest and genome maintenance. Genes Dev 17, 615–628. 10.1101/gad.1067403. [PubMed: 12629044]

10. Eykelenboom JK, Harte EC, Canavan L, Pastor-Peidro A, Calvo-Asensio I, Llorens-Agost M, and Lowndes NF (2013). ATR activates the S-M checkpoint during unperturbed growth to ensure sufficient replication prior to mitotic onset. Cell Rep 5, 1095–1107. 10.1016/j.celrep.2013.10.027. [PubMed: 24268773]

11. Buisson R, Boisvert JL, Benes CH, and Zou L (2015). Distinct but Concerted Roles of ATR, DNA-PK, and Chk1 in Countering Replication Stress during S Phase. Mol Cell 59, 1011–1024. 10.1016/j.molcel.2015.07.029. [PubMed: 26365377]

12. Kumar A, Mazzanti M, Mistrik M, Kosar M, Beznoussenko GV, Mironov AA, Garre M, Parazzoli D, Shivashankar GV, Scita G, et al. (2014). ATR mediates a checkpoint at the nuclear envelope in response to mechanical stress. Cell 158, 633–646. 10.1016/j.cell.2014.05.046. [PubMed: 25083873]

13. Sansregret L, and Swanton C (2017). The Role of Aneuploidy in Cancer Evolution. Cold Spring Harb Perspect Med 7. 10.1101/cshperspect.a028373.

14. Agustinus AS, Al-Rawi D, Dameracharla B, Raviram R, Jones BSCL, Stransky S, Scipioni L, Luebeck J, Di Bona M, Norkunaite D, et al. (2023). Epigenetic dysregulation from chromosomal transit in micronuclei. Nature. 10.1038/s41586-023-06084-7.

15. Papathanasiou S, Mynhier NA, Liu S, Brunette G, Stokasimov E, Jacob E, Li L, Comenho C, van Steensel B, Buenrostro JD, et al. (2023). Heritable transcriptional defects from aberrations of nuclear architecture. Nature. 10.1038/s41586-023-06157-7.

16. Zhang CZ, Spektor A, Cornils H, Francis JM, Jackson EK, Liu S, Meyerson M, and Pellman D (2015). Chromothripsis from DNA damage in micronuclei. Nature 522, 179–184. 10.1038/nature14493. [PubMed: 26017310]

17. Liu S, Kwon M, Mannino M, Yang N, Renda F, Khodjakov A, and Pellman D (2018). Nuclear envelope assembly defects link mitotic errors to chromothripsis. Nature 561, 551–555. 10.1038/s41586-018-0534-z. [PubMed: 30232450]

18. Hatch EM, Fischer AH, Deerinck TJ, and Hetzer MW (2013). Catastrophic nuclear envelope collapse in cancer cell micronuclei. Cell 154, 47–60. 10.1016/j.cell.2013.06.007. [PubMed: 23827674]

19. Mackenzie KJ, Carroll P, Martin CA, Murina O, Fluteau A, Simpson DJ, Olova N, Sutcliffe H, Rainger JK, Leitch A, et al. (2017). cGAS surveillance of micronuclei links genome instability to innate immunity. Nature 548, 461–465. 10.1038/nature23449. [PubMed: 28738408]

20. Harding SM, Benci JL, Irianto J, Discher DE, Minn AJ, and Greenberg RA (2017). Mitotic progression following DNA damage enables pattern recognition within micronuclei. Nature 548, 466–470. 10.1038/nature23470. [PubMed: 28759889]

21. Yang H, Wang H, Ren J, Chen Q, and Chen ZJ (2017). cGAS is essential for cellular senescence. Proc Natl Acad Sci U S A 114, E4612–E4620. 10.1073/pnas.1705499114. [PubMed: 28533362]

22. Gui X, Yang H, Li T, Tan X, Shi P, Li M, Du F, and Chen ZJ (2019). Autophagy induction via STING trafficking is a primordial function of the cGAS pathway. Nature 567, 262–266. 10.1038/s41586-019-1006-9. [PubMed: 30842662]

23. Kwon J, and Bakhoum SF (2020). The Cytosolic DNA-Sensing cGAS-STING Pathway in Cancer. Cancer Discov 10, 26–39. 10.1158/2159-8290.CD-19-0761. [PubMed: 31852718]

24. Mohr L, Toufektchan E, von Morgen P, Chu K, Kapoor A, and Maciejowski J (2021). ER-directed TREX1 limits cGAS activation at micronuclei. Mol Cell 81, 724–738 e729. 10.1016/j.molcel.2020.12.037. [PubMed: 33476576]

25. Rello-Varona S, Lissa D, Shen S, Niso-Santano M, Senovilla L, Marino G, Vitale I, Jemaa M, Harper F, Pierron G, et al. (2012). Autophagic removal of micronuclei. Cell Cycle 11, 170–176. 10.4161/cc.11.1.18564. [PubMed: 22185757]

26. Zhao M, Wang F, Wu J, Cheng Y, Cao Y, Wu X, Ma M, Tang F, Liu Z, Liu H, and Ge B (2021). CGAS is a micronucleophagy receptor for the clearance of micronuclei. Autophagy, 1–17. 10.1080/15548627.2021.1899440.
27. Bakhoum SF, Thompson SL, Manning AL, and Compton DA (2009). Genome stability is ensured by temporal control of kinetochore-microtubule dynamics. Nat Cell Biol 11, 27–35. 10.1038/ncb1809. [PubMed: 19060894]
28. Frattini A, Fabbri M, Valli R, De Paoli E, Montalbano G, Gribaldo L, Pasquali F, and Maserati E (2015). High variability of genomic instability and gene expression profiling in different HeLa clones. Sci Rep 5, 15377. 10.1038/srep15377. [PubMed: 26483214]
29. Yoon DS, Wersto RP, Zhou W, Chrest FJ, Garrett ES, Kwon TK, and Gabrielson E (2002). Variable levels of chromosomal instability and mitotic spindle checkpoint defects in breast cancer. Am J Pathol 161, 391–397. 10.1016/s0002-9440(10)64194-6. [PubMed: 12163363]
30. Ganem NJ, Godinho SA, and Pellman D (2009). A mechanism linking extra centrosomes to chromosomal instability. Nature 460, 278–282. 10.1038/nature08136. [PubMed: 19506557]
31. Ly P, Teitz LS, Kim DH, Shoshani O, Skaletsky H, Fachinetti D, Page DC, and Cleveland DW (2017). Selective Y centromere inactivation triggers chromosome shattering in micronuclei and repair by non-homologous end joining. Nat Cell Biol 19, 68–75. 10.1038/ncb3450. [PubMed: 27918550]
32. Bakhoum SF, Ngo B, Laughney AM, Cavallo JA, Murphy CJ, Ly P, Shah P, Sriram RK, Watkins TBK, Taunk NK, et al. (2018). Chromosomal instability drives metastasis through a cytosolic DNA response. Nature 553, 467–472. 10.1038/nature25432. [PubMed: 29342134]
33. Moore AT., Rankin KE., von Dassow G., Peris L., Wagenbach M., Ovechkina Y., Andrieux A., Job D., and Wordeman L. (2005). MCAK associates with the tips of polymerizing microtubules. Journal of Cell Biology 169, 391–397. 10.1083/jcb.200411089. [PubMed: 15883193]
34. Chen J, Harding SM, Natesan R, Tian L, Benci JL, Li W, Minn AJ, Asangani IA, and Greenberg RA (2020). Cell Cycle Checkpoints Cooperate to Suppress DNA- and RNA-Associated Molecular Pattern Recognition and Anti-Tumor Immune Responses. Cell Rep 32, 108080. 10.1016/j.celrep.2020.108080. [PubMed: 32877684]
35. Bartkova J, Rezaei N, Liontos M, Karakaidos P, Kletsas D, Issaeva N, Vassiliou LV, Kolettas E, Niforou K, Zoumpourlis VC, et al. (2006). Oncogene-induced senescence is part of the tumorigenesis barrier imposed by DNA damage checkpoints. Nature 444, 633–637. 10.1038/nature05268. [PubMed: 17136093]
36. Vargas JD, Hatch EM, Anderson DJ, and Hetzer MW (2012). Transient nuclear envelope rupturing during interphase in human cancer cells. Nucleus 3, 88–100. 10.4161/nucl.18954. [PubMed: 22567193]
37. Crasta K, Ganem NJ, Dagher R, Lantermann AB, Ivanova EV, Pan Y, Nezi L, Protopopov A, Chowdhury D, and Pellman D (2012). DNA breaks and chromosome pulverization from errors in mitosis. Nature 482, 53–58. 10.1038/nature10802. [PubMed: 22258507]
38. Heald R, and McKeon F (1990). Mutations of phosphorylation sites in lamin A that prevent nuclear lamina disassembly in mitosis. Cell 61, 579–589. 10.1016/0092-8674(90)90470-y. [PubMed: 2344612]
39. Ward GE, and Kirschner MW (1990). Identification of cell cycle-regulated phosphorylation sites on nuclear lamin C. Cell 61, 561–577. 10.1016/0092-8674(90)90469-u. [PubMed: 2188730]
40. Peter M, Nakagawa J, Doree M, Labbe JC, and Nigg EA (1990). In vitro disassembly of the nuclear lamina and M phase-specific phosphorylation of lamins by cdc2 kinase. Cell 61, 591–602. 10.1016/0092-8674(90)90471-p. [PubMed: 2188731]
41. Hochegger H, Dejsuphong D, Sonoda E, Saberi A, Rajendra E, Kirk J, Hunt T, and Takeda S (2007). An essential role for Cdk1 in S phase control is revealed via chemical genetics in vertebrate cells. J Cell Biol 178, 257–268. 10.1083/jcb.200702034. [PubMed: 17635936]
42. Pines J, and Hunter T (1991). Human cyclins A and B1 are differentially located in the cell and undergo cell cycle-dependent nuclear transport. J Cell Biol 115, 1–17. 10.1083/jcb.115.1.1. [PubMed: 1717476]

43. Kochin V, Shimi T, Torvaldson E, Adam SA, Goldman A, Pack CG, Melo-Cardenas J, Imanishi SY, Goldman RD, and Eriksson JE (2014). Interphase phosphorylation of lamin A. J Cell Sci 127, 2683–2696. 10.1242/jcs.141820. [PubMed: 24741066]
44. Stokes MP, Rush J, Macneill J, Ren JM, Sprott K, Nardone J, Yang V, Beausoleil SA, Gygi SP, Livingstone M, et al. (2007). Profiling of UV-induced ATM/ATR signaling pathways. Proc Natl Acad Sci U S A 104, 19855–19860. 10.1073/pnas.0707579104. [PubMed: 18077418]
45. Li T, and Chen ZJ (2018). The cGAS-cGAMP-STING pathway connects DNA damage to inflammation, senescence, and cancer. J Exp Med 215, 1287–1299. 10.1084/jem.20180139. [PubMed: 29622565]
46. Suter MA, Tan NY, Thiam CH, Khatoo M, MacAry PA, Angeli V, Gasser S, and Zhang YL (2021). cGAS-STING cytosolic DNA sensing pathway is suppressed by JAK2-STAT3 in tumor cells. Sci Rep 11, 7243. 10.1038/s41598-021-86644-x. [PubMed: 33790360]
47. Yang H, Wang H, Ren J, Chen Q, and Chen ZJ (2017). cGAS is essential for cellular senescence. Proceedings of the National Academy of Sciences 114, E4612–E4620. doi:10.1073/pnas.1705499114.
48. Kuilman T, Michaloglou C, Vredeveld LC, Douma S, van Doorn R, Desmet CJ, Aarden LA, Mooi WJ, and Peeper DS (2008). Oncogene-induced senescence relayed by an interleukin-dependent inflammatory network. Cell 133, 1019–1031. 10.1016/j.cell.2008.03.039. [PubMed: 18555778]
49. Itakura E, and Mizushima N (2011). p62 Targeting to the autophagosome formation site requires self-oligomerization but not LC3 binding. J Cell Biol 192, 17–27. 10.1083/jcb.201009067. [PubMed: 21220506]
50. Deschamps T, and Kalamvoki M (2017). Impaired STING Pathway in Human Osteosarcoma U2OS Cells Contributes to the Growth of ICP0-Null Mutant Herpes Simplex Virus. J Virol 91. 10.1128/JVI.00006-17.
51. Barroso-Gonzalez J, Garcia-Exposito L, Hoang SM, Lynskey ML, Roncaioli JL, Ghosh A, Wallace CT, de Vitis M, Modesti M, Bernstein KA, et al. (2019). RAD51AP1 Is an Essential Mediator of Alternative Lengthening of Telomeres. Mol Cell 76, 11–26 e17. 10.1016/j.molcel.2019.06.043. [PubMed: 31400850]
52. Santaguida S, Richardson A, Iyer DR, M'Saad O, Zasadil L, Knouse KA, Wong YL, Rhind N, Desai A, and Amon A (2017). Chromosome Mis-segregation Generates Cell-Cycle-Arrested Cells with Complex Karyotypes that Are Eliminated by the Immune System. Dev Cell 41, 638–651 e635. 10.1016/j.devcel.2017.05.022. [PubMed: 28633018]
53. Marcus A, Mao AJ, Lensink-Vasan M, Wang L, Vance RE, and Raulet DH (2018). Tumor-Derived cGAMP Triggers a STING-Mediated Interferon Response in Non-tumor Cells to Activate the NK Cell Response. Immunity 49, 754–763 e754. 10.1016/j.immuni.2018.09.016. [PubMed: 30332631]
54. Zou L, and Elledge SJ (2003). Sensing DNA damage through ATRIP recognition of RPA-ssDNA complexes. Science 300, 1542–1548. 10.1126/science.1083430. [PubMed: 12791985]
55. Byun TS, Pacek M, Yee MC, Walter JC, and Cimprich KA (2005). Functional uncoupling of MCM helicase and DNA polymerase activities activates the ATR-dependent checkpoint. Genes Dev 19, 1040–1052. 10.1101/gad.1301205. [PubMed: 15833913]
56. Shiotani B, and Zou L (2009). Single-stranded DNA orchestrates an ATM-to-ATR switch at DNA breaks. Mol Cell 33, 547–558. 10.1016/j.molcel.2009.01.024. [PubMed: 19285939]
57. MacDougall CA, Byun TS, Van C, Yee MC, and Cimprich KA (2007). The structural determinants of checkpoint activation. Genes Dev 21, 898–903. 10.1101/gad.1522607. [PubMed: 17437996]
58. Bass TE, Luzwick JW, Kavanaugh G, Carroll C, Dungrawala H, Glick GG, Feldkamp MD, Putney R, Chazin WJ, and Cortez D (2016). ETAA1 acts at stalled replication forks to maintain genome integrity. Nat Cell Biol 18, 1185–1195. 10.1038/ncb3415. [PubMed: 27723720]
59. Haahr P, Hoffmann S, Tollenaere MA, Ho T, Toledo LI, Mann M, Bekker-Jensen S, Raschle M, and Mailand N (2016). Activation of the ATR kinase by the RPA-binding protein ETAA1. Nat Cell Biol 18, 1196–1207. 10.1038/ncb3422. [PubMed: 27723717]
60. Bass TE, and Cortez D (2019). Quantitative phosphoproteomics reveals mitotic function of the ATR activator ETAA1. J Cell Biol 218, 1235–1249. 10.1083/jcb.201810058. [PubMed: 30755469]

61. Bekker-Jensen S, Lukas C, Kitagawa R, Melander F, Kastan MB, Bartek J, and Lukas J (2006). Spatial organization of the mammalian genome surveillance machinery in response to DNA strand breaks. J Cell Biol 173, 195–206. 10.1083/jcb.200510130. [PubMed: 16618811]

62. Petermann E, and Caldecott KW (2006). Evidence that the ATR/Chk1 pathway maintains normal replication fork progression during unperturbed S phase. Cell Cycle 5, 2203–2209. 10.4161/cc.5.19.3256. [PubMed: 16969104]

63. Petermann E, Woodcock M, and Helleday T (2010). Chk1 promotes replication fork progression by controlling replication initiation. Proc Natl Acad Sci U S A 107, 16090–16095. 10.1073/pnas.1005031107. [PubMed: 20805465]

64. Kidiyoor GR, Li Q, Bastianello G, Bruhn C, Giovannetti I, Mohamood A, Beznoussenko GV, Mironov A, Raab M, Piel M, et al. (2020). ATR is essential for preservation of cell mechanics and nuclear integrity during interstitial migration. Nat Commun 11, 4828. 10.1038/s41467-020-18580-9. [PubMed: 32973141]

65. Coppé JP, Desprez PY, Krtolica A, and Campisi J (2010). The senescence-associated secretory phenotype: the dark side of tumor suppression. Annu Rev Pathol 5, 99–118. 10.1146/annurev-pathol-121808-102144. [PubMed: 20078217]

66. Decout A, Katz JD, Venkatraman S, and Ablasser A (2021). The cGAS–STING pathway as a therapeutic target in inflammatory diseases. Nature Reviews Immunology 21, 548–569. 10.1038/s41577-021-00524-z.

67. Tang S, Stokasimov E, Cui Y, and Pellman D (2022). Breakage of cytoplasmic chromosomes by pathological DNA base excision repair. Nature 606, 930–936. 10.1038/s41586-022-04767-1. [PubMed: 35477155]

68. Petermann E, Maya-Mendoza A, Zachos G, Gillespie DA, Jackson DA, and Caldecott KW (2006). Chk1 requirement for high global rates of replication fork progression during normal vertebrate S phase. Mol Cell Biol 26, 3319–3326. 10.1128/MCB.26.8.3319-3326.2006. [PubMed: 16581803]

69. Feng X, Tubbs A, Zhang C, Tang M, Sridharan S, Wang C, Jiang D, Su D, Zhang H, Chen Z, et al. (2020). ATR inhibition potentiates ionizing radiation-induced interferon response via cytosolic nucleic acid-sensing pathways. EMBO J 39, e104036. 10.15252/embj.2019104036. [PubMed: 32484965]

Highlights

- ATR promotes rupture of Lamin B-negative MN during S phase
- ATR phosphorylates Lamin A/C at S395 and primes S392 for CDK1 phosphorylation
- ATRi decreases cGAS and autophagy-mediated clearance of micronuclear DNA
- ATRi reduces cGAS and NK cell-mediated clearance of MN-bearing cells

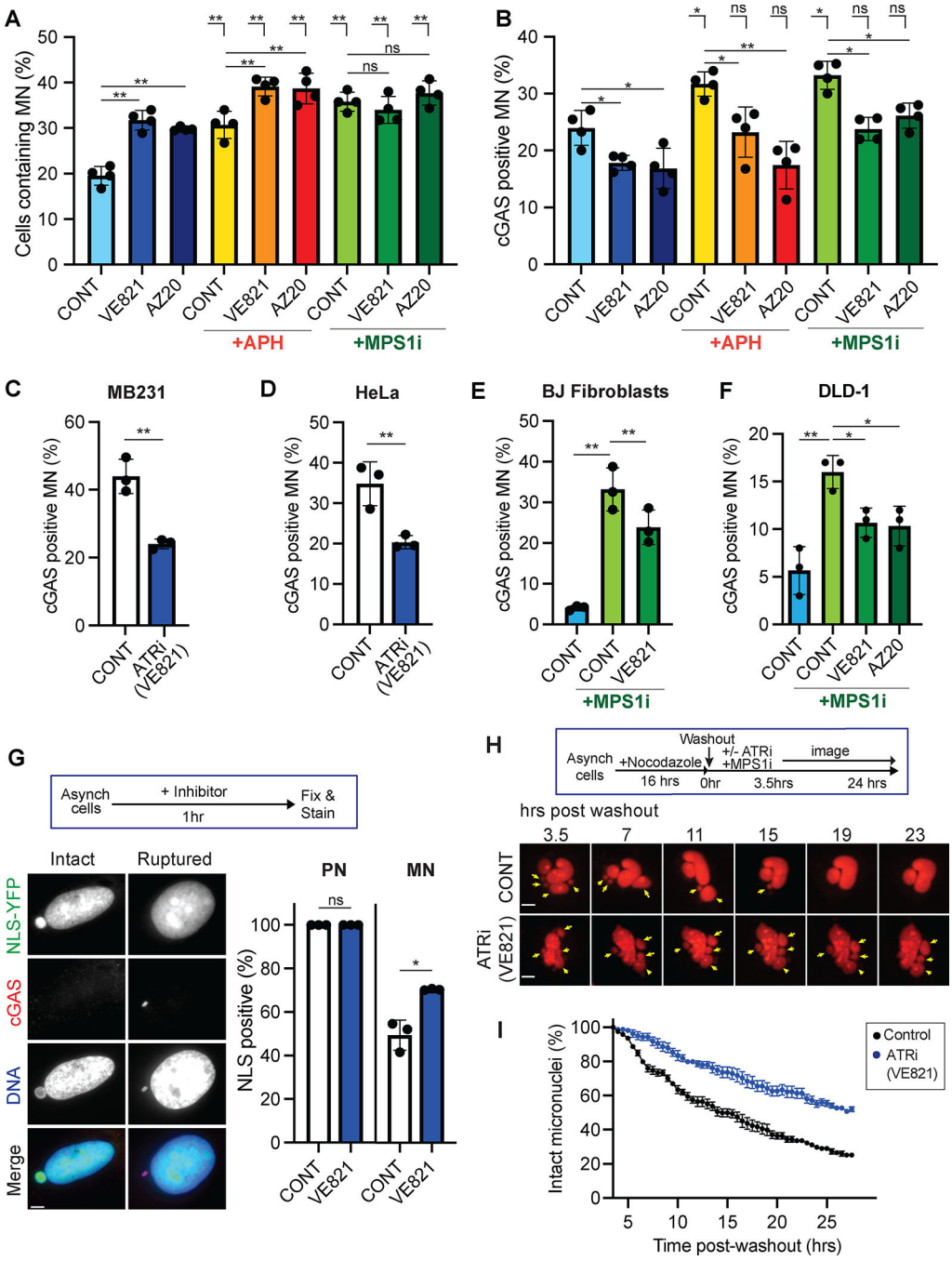

Figure 1. ATR inhibition reduces MN rupture

(A) Percentage of U2OS cells containing MN after mock treatment (CONT) or treatment with ATRi (VE-821, AZ20), APH (aphidicolin), MPS1i (reversine), ATRi and APH, or ATRi and MPS1i for 24 hours (>300 MN analyzed per condition).

(B) Percentage of cGAS^{+} MN in U2OS cells after mock treatment (CONT) or treatment with ATRi (VE-821, AZ20), APH, MPS1i, or their combinations for 24 hours (>300 MN analyzed per condition).

(**C-D**) Percentage of cGAS$^+$ MN in MDA-MB-231 (C) and HeLa (D) cells after 24 hours of mock (CONT) or ATRi (VE-821) treatment.
(**E-F**) Percentage of cGAS$^+$ MN in BJ Fibroblast (E) and DLD-1 (F) cells after 24 hours of mock (CONT), MPS1i, or ATRi treatment.
(G) (Left) Images of NLS-YFP-expressing and MN-containing U2OS cells stained for cGAS (red) and DNA (blue). (Right) Quantification of the NLS-YFP$^+$ MN or PN in mock or ATRi-treated U2OS cells. Cells were treated with ATRi for 1 hour (>100 MN analyzed per condition).
(H) Live-cell imaging of NLS-YFP-expressing U2OS cells after mock (CONT) or ATRi treatment. Cells were arrested in mitosis with Nocodazole and then released in MPS1i. Imaging started 3.5 hours post-release and continued until 27 hours post-release.
(I) Fraction of intact MN in U2OS cells over time measured by the presence of NLS-RFP in MN [average from 3 live-cell imaging experiments in (H)].
Error bars in all panels represent SEM. *P ≤ 0.05, **P ≤ 0.01, ANOVA with multiple comparisons with Tukey's correction was performed for panels comparing more than 2 conditions. Two-tailed *t*-test was used for panels with only two conditions. Scale bar: 10 μm.

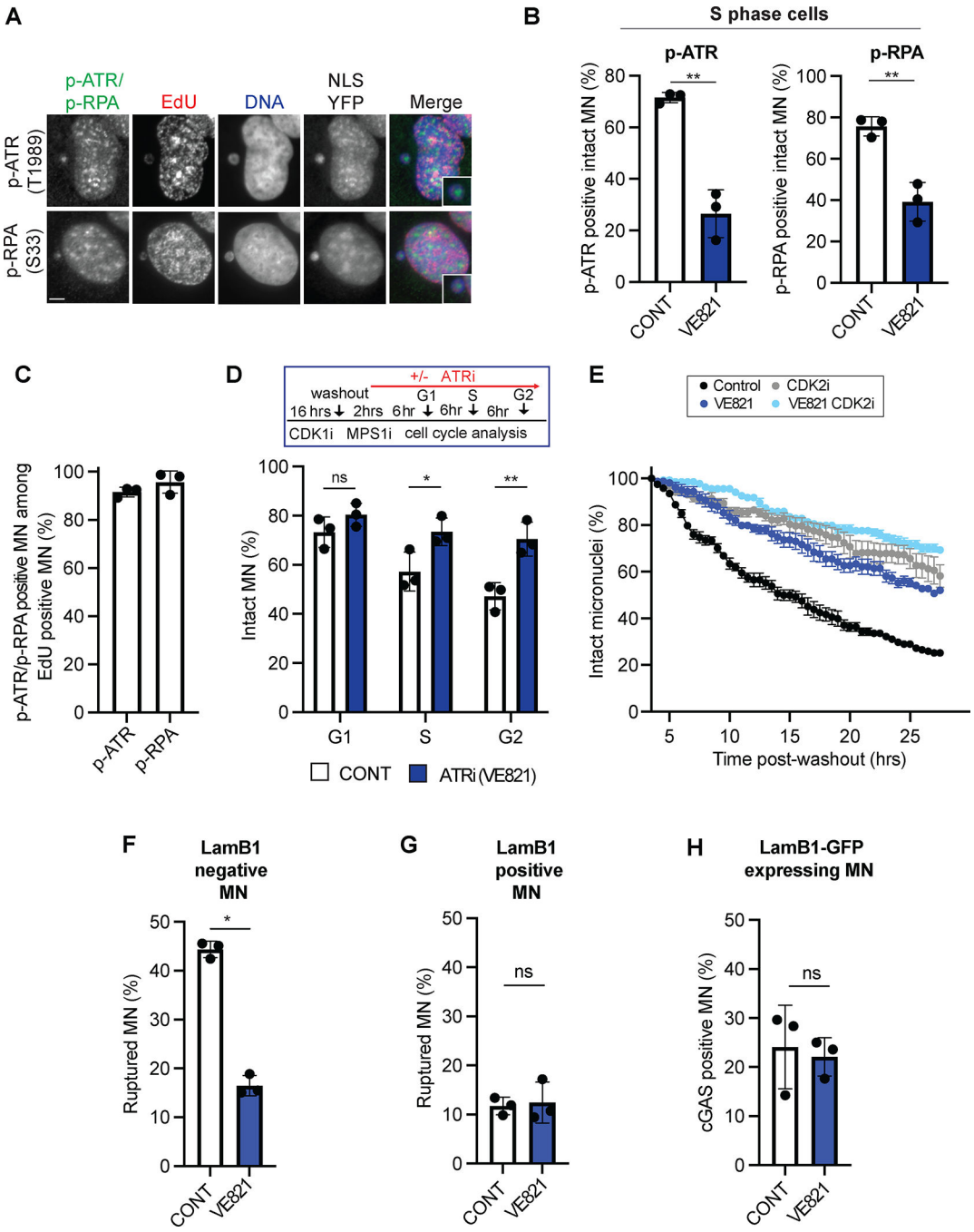

Figure 2. ATR is active in micronuclei during S phase to promote rupture

(**A**) NLS-YFP-expressing U2OS cells in S phase were labeled with EdU for 1 hour, immunostained for p-ATR or p-RPA32, and DAPI-stained for DNA.

(**B**) Percentage of MN positive for p-ATR (left) or p-RPA32 (right) in S phase U2OS cells untreated (CONT) or treated with ATRi for 1 hour (>60 MN per condition).

(**C**) Percentage of MN positive for both p-ATR and EdU or both p-RPA32 and EdU in asynchronously growing U2OS cells.

(**D**) Percentage of intact MN in untreated (CONT) or ATRi-treated U2OS cells in G1, S, and G2 phase. Cells were arrested in G2/M with CDK1i and then released into mitosis in MPS1i. Additional inhibitors were added 2 hours after CDK1i washout. G1, S, and G2 phase cells were isolated 8, 14, and 20 hours post-release, respectively. DAPI and EdU intensities for each cell were analyzed to identify cells in G1, S, and G2 (>40 MN per condition per replicate).

(**E**) Fraction of intact MN in NLS-RFP-expressing U2OS cells from live-cell imaging following Nocodazole block-and-release in mitosis. Cells were released from Nocodazole in MPS1i, and ATRi, CDK2i, or both were added 2 hours post-release. Imaging started 3.5 hours post-release and continued until 27 hours post-release (>60 MN were analyzed per experiment).

(**F-G**) Percentage of ruptured MN among Lamin $B1^{-}$ (F) and Lamin $B1^{+}$ (G) MN in U2OS cells. Cells were either untreated (CONT) or treated with ATRi for 1 hour.

(**H**) Percentage of $cGAS^{+}$ MN in Lamin B1-GFP-expressing U2OS cells untreated (CONT) or treated with ATRi for 1 hour.

Error bars in all panels represent SEM. *P ≤ 0.05, **P ≤ 0.01, ANOVA with multiple comparisons with Tukey's correction was performed for panels comparing more than 2 conditions. Two-tailed *t*-test was used for panels with only two conditions. Scale bar: 10 μm.

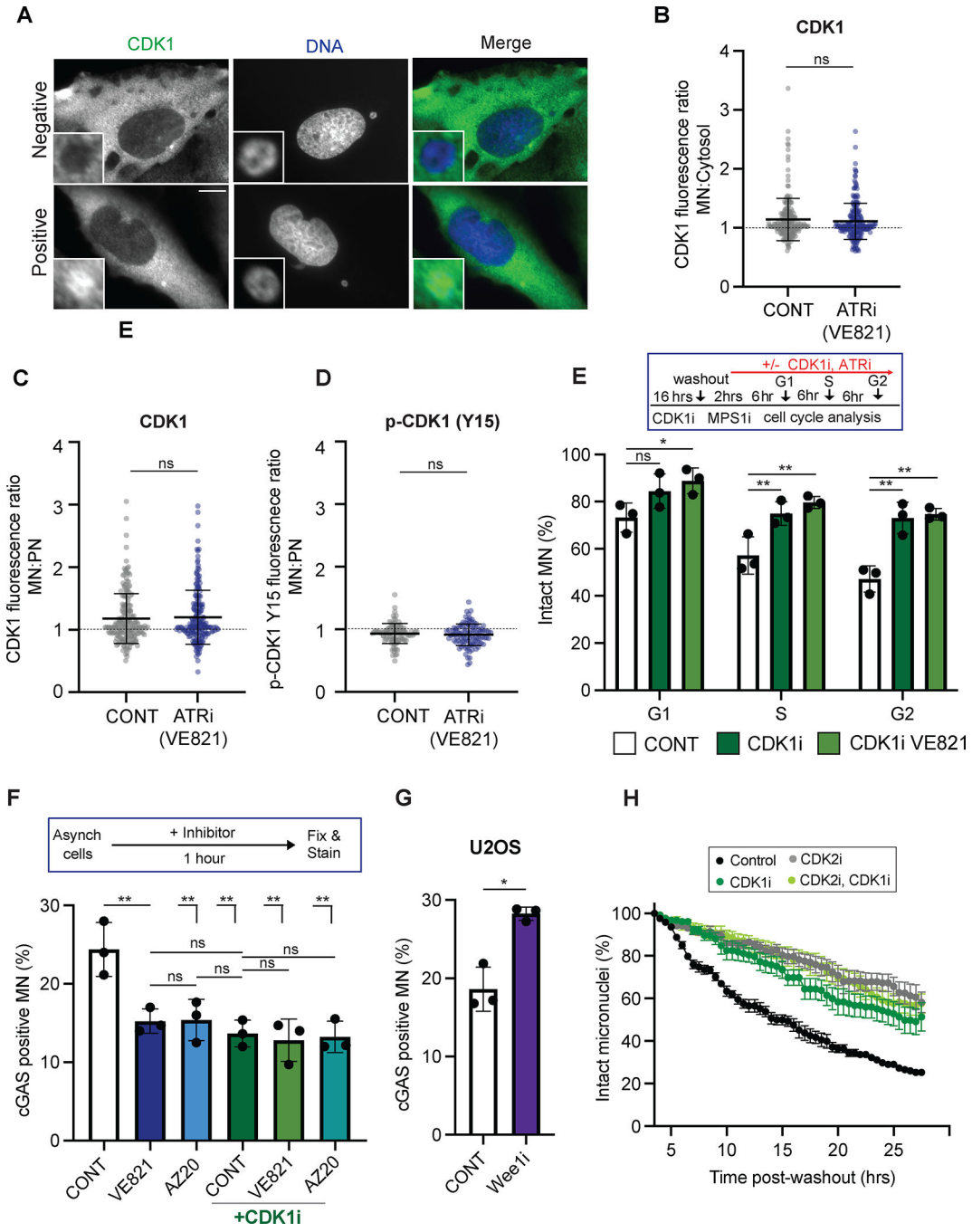

Figure 3. CDK1 activity is essential for MN rupture in S phase.

(A) Images of MN positive or negative for CDK1 in U2OS cells. Cells were DAPI-stained for DNA to identify MN.

(**B-C**) Ratios of average CDK1 fluorescence between MN and cytosol (B) or between MN and PN (C) in the same cells. U2OS cells were untreated (CONT) or treated with ATRi for 1 hour (>100 cells per condition).

(**D**) Ratios of average p-CDK1 Y15 fluorescence between MN and PN in the same cells.

(**E**) Percentage of intact MN following CDK1i block-and-release in different cell cycle phases. Cells were arrested in G2/M with CDK1i and then released into mitosis in MPS1i. CDK1i or ATRi was added 2 hours after release. G1, S, and G2 phase cells were isolated 8, 14, and 20 hours post-release, respectively (>40 MN per condition).
(**F**) Percentages of $cGAS^+$ MN in untreated (CONT), ATRi-treated (VE-821, AZ20), or ATRi and CDK1i-treated U2OS cells. Asynchronous cells were treated with inhibitor for 1 hour.
(**G**) Percentage of $cGAS^+$ MN in untreated (CONT) or Wee1i (2μM MK1775) treated U2OS cells.
(**H**) Fraction of intact MN in NLS-RFP-expressing U2OS cells from live-cell imaging following nocodazole block-and-release in mitosis. Cells were released from Nocodazole in MPS1i, and CDK1i, CDK2i, or both were added 2 hours post-release. Imaging started 3.5 hours post-release and continued until 27 hours post-release (>60 MN were analyzed per experiment).
All experiments were done in 3 biological replicates (n=3). Error bars in panels (E) and (F) represent SDM. *P ≤ 0.05, **P ≤ 0.01, two-tailed *t*-test. Error bars in all other panels represent SEM. *P ≤ 0.05, **P ≤ 0.01, ANOVA with multiple comparisons with Tukey's correction was performed for panels comparing more than 2 conditions. Two-tailed *t*-test was used for panels with only two conditions. Scale bar: 10 μm.

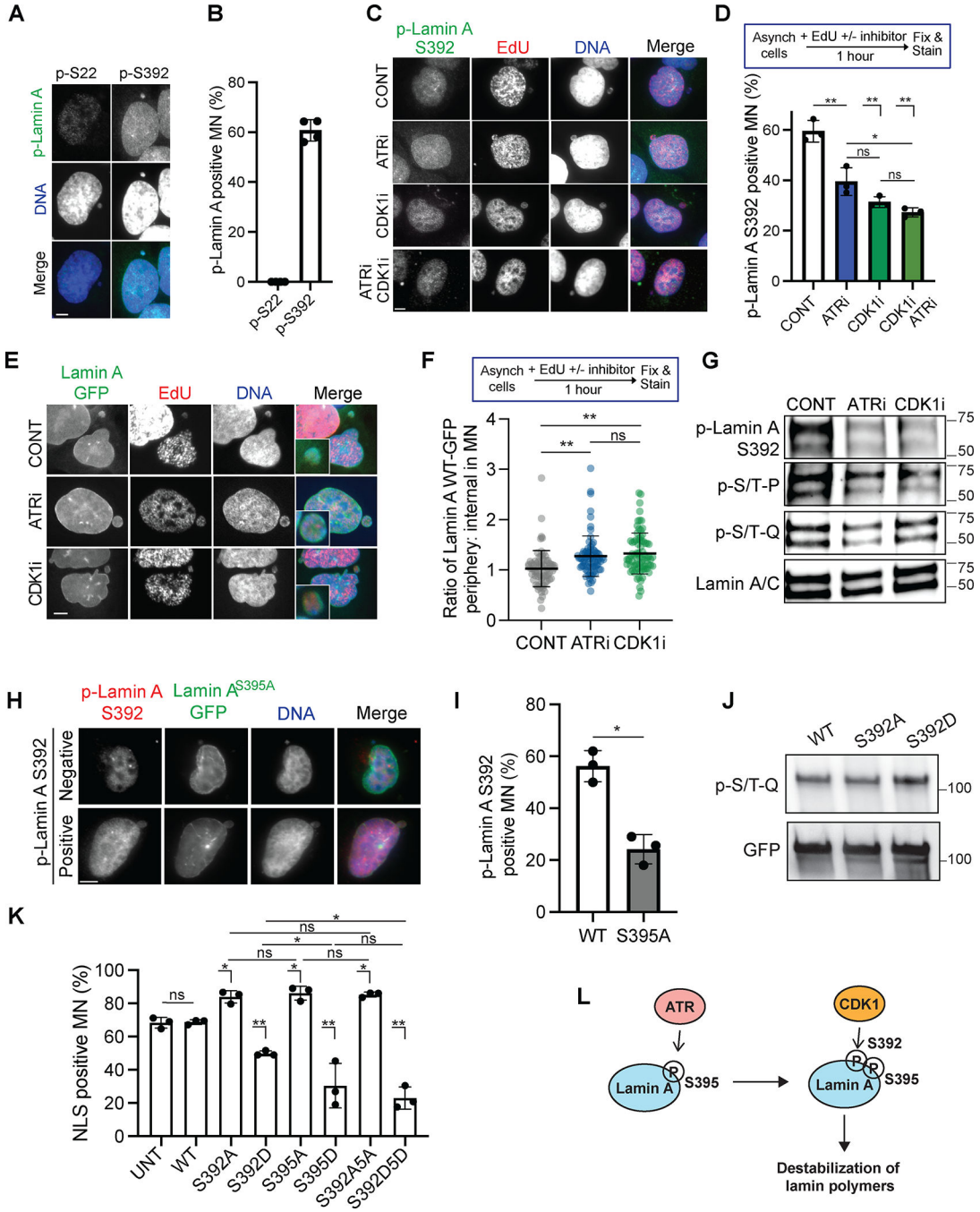

Figure 4. ATR primes Lamin A/C for CDK1 phosphorylation.

(**A**) Images of MN-containing U2OS cells immunostained for p-Lamin A S22 or p-Lamin A S392 and DAPI-stained for DNA.

(**B**) Percentage of MN positive for p-Lamin A S22 or p-Lamin A S392 in untreated U2OS cells.

(**C**) Images of MN-containing U2OS cells untreated (CONT) or treated with ATRi, CDK1i, or both. Cells were labeled with EdU and simultaneously treated with inhibitors for 1 hour, and then immunostained for p-Lamin A S392 and DAPI-stained for DNA.

(**D**) Percentage of p-Lamin A S392^{+} MN in S-phase U2OS cells.
(**E**) Images of Lamin A-GFP-expressing and MN-containing U2OS cells untreated (CONT) or treated with ATRi or CDK1i. Cells were labeled with EdU and simultaneously treated with inhibitors for 1 hour, and then immunostained for GFP and DAPI-stained for DNA.
(**F**) Fluorescence ratio of Lamin WT-GFP signals at the periphery (membrane) of MN versus the interior of MN for U2OS cells expressing Lamin A WT-GFP. Cells were untreated (CONT) or treated with ATRi or CDK1i and simultaneously labeled with EdU for 1 hour (>50 cells analyzed per condition).
(**G**) U2OS cells untreated (CONT) or treated with ATRi or CDK1i were used for Lamin A/C immunoprecipitation. Immunoprecipitates were analyzed with phospho-specific antibodies recognizing the CDK consensus motif (p-S/T-P) and the ATR consensus motif (p-S/T-Q). Immunoprecipitated Lamin A/C were used as loading controls.
(**H**) U2OS cells expressing Lamin A^{S395A}-GFP were immunostained for p-Lamin A (S392) and DAPI-stained for DNA. The positive or negative status of p-Lamin A signals was determined using an arbitrary threshold.
(**I**) Percentage of MN positive for p-Lamin A S392 in U2OS cells expressing Lamin A^{WT}-GFP or Lamin A^{S395A}-GFP.
(**J**) Immunoblot of the ATR consensus motif (p-S/T-Q) in cells expressing Lamin A^{WT}-GFP, Lamin A^{S392A}-GFP, or Lamin A^{S392D}-GFP. GFP signals of the fusion proteins were used as loading controls.
(**K**) Percentage of YFP^{+} MN in U2OS cells co-expressing NLS-YFP and one of the seven indicated Lamin A-GFP variants. The positive or negative status of YFP signals was determined using an arbitrary threshold.
(**L**) A summary schematic.
Error bars in all panels represent SEM. *P ≤ 0.05, **P ≤ 0.01, ANOVA with multiple comparisons with Tukey's correction was performed for panels comparing more than 2 conditions. Two-tailed *t*-test was used for panels with only two conditions. Scale bar: 10 μm.

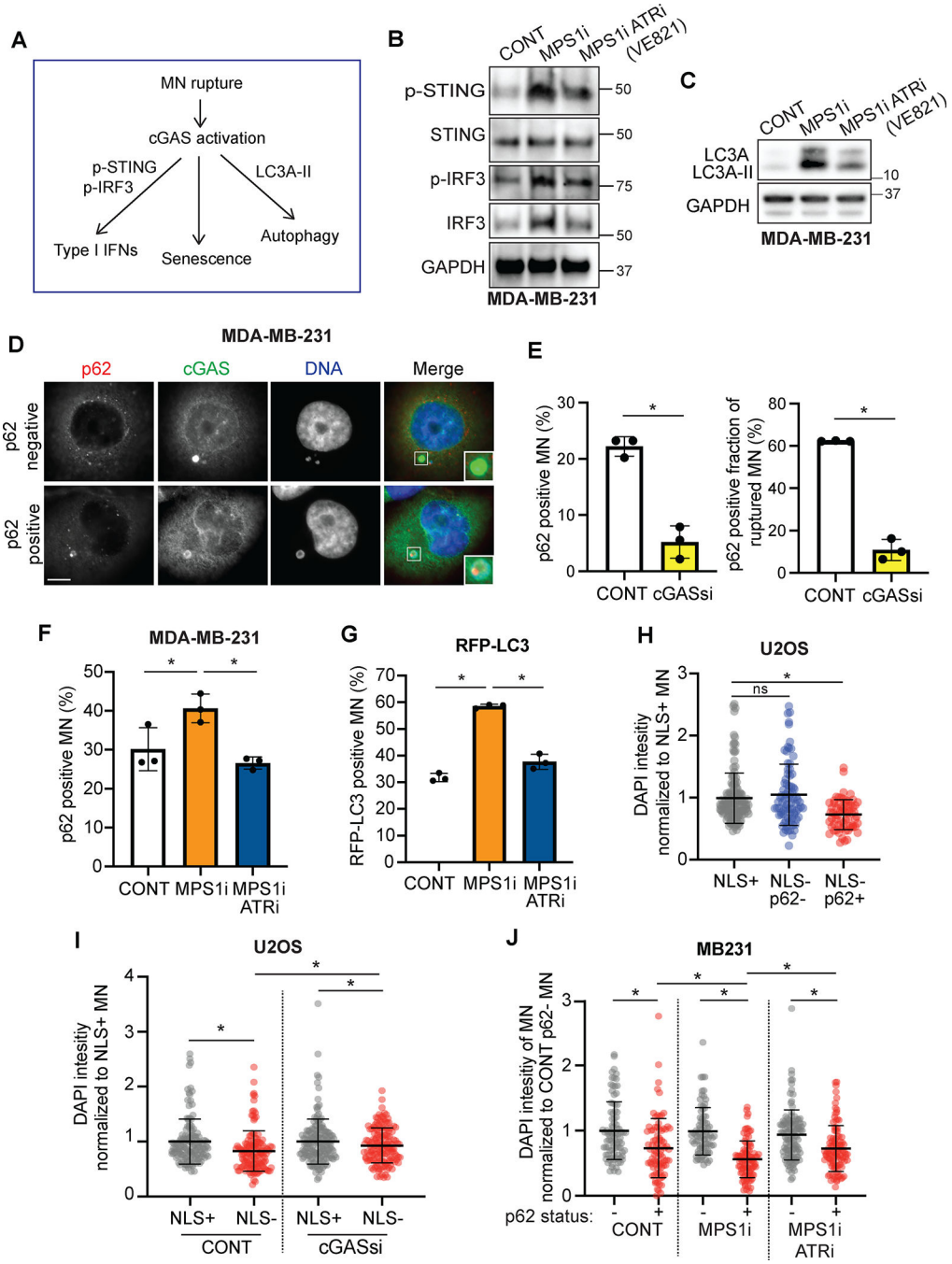

Figure 5. ATR promotes MN-induced cGAS activation.

(**A**) A diagram of MN rupture-triggered downstream pathways.

(**B-C**) Immunoblots of markers of cGAS-mediated signals [p-STING, STING, p-IRF3, IRF3 in (B)] and autophagy [LC3A in (C)] in MDA-MB-231 cells untreated (CONT) or treated with MPS1i or MPS1i and ATRi for 24 hours. GAPDH serves as a loading control.

(**D**) Images of MDA-MB-231 cells immunostained for p62 and cGAS and DAPI-stained for DNA. The positive or negative status of p62 was determined using an arbitrary threshold.

(**E**) (Left) Percentage of $p62^+$ MN in MDA-MB-231 cells treated with control or cGAS siRNA. (Right) Percentage of $p62^+$ MN among ruptured MN in cells treated with control or cGAS siRNA. Cells were fixed and stained 2 days post-siRNA transfection. MN rupture was determined by presence of NLS-YFP in MN (>100 cells per condition).
(**F**) Percentage of $p62^+$ MN in MDA-MB-231 cells untreated (CONT) or treated with MPS1i or MSP1i and ATRi for 24 hours (>100 cells per condition).
(**G**) Percentage of LC3-RFP^+ MN in MDA-MB-231 cells expressing LC3-RFP. Cells were untreated (CONT) or treated with MPS1i or MPS1i and ATRi for 24 hours. LC3-RFP^+ MN were determined by presence of RFP in MN (>100 MN per condition).
(**H**) Normalized average DAPI fluorescence intensities in the indicated MN subpopulations in NLS-YFP-expressing U2OS cells. All measured DAPI intensities were normalized to the average in the NLS^+ condition (>80 cells per condition).
(**I**) Normalized average DAPI fluorescence intensities in the indicated MN subpopulations in U2OS cells treated with control or cGAS siRNA. All measured DAPI intensities were normalized to the average in the NLS^+ conditions (>80 cells per condition).
(**J**) Average DAPI intensity in MN of MDA-MB-231 cells untreated (CONT), treated with MPS1i for 24 hours, or treated with MPS1i for 24 hours and then with ATRi (VE-821) for 1 hour. All measurements were normalized to the average in the CONT $p62^-$ condition (>100 cells per condition).
Error bars in all panels represent SEM. *P ≤ 0.05, **P ≤ 0.01, ANOVA with multiple comparisons with Tukey's correction was performed for panels comparing more than 2 conditions. Two-tailed *t*-test was used for panels with only two conditions. Scale bar: 10 μm.

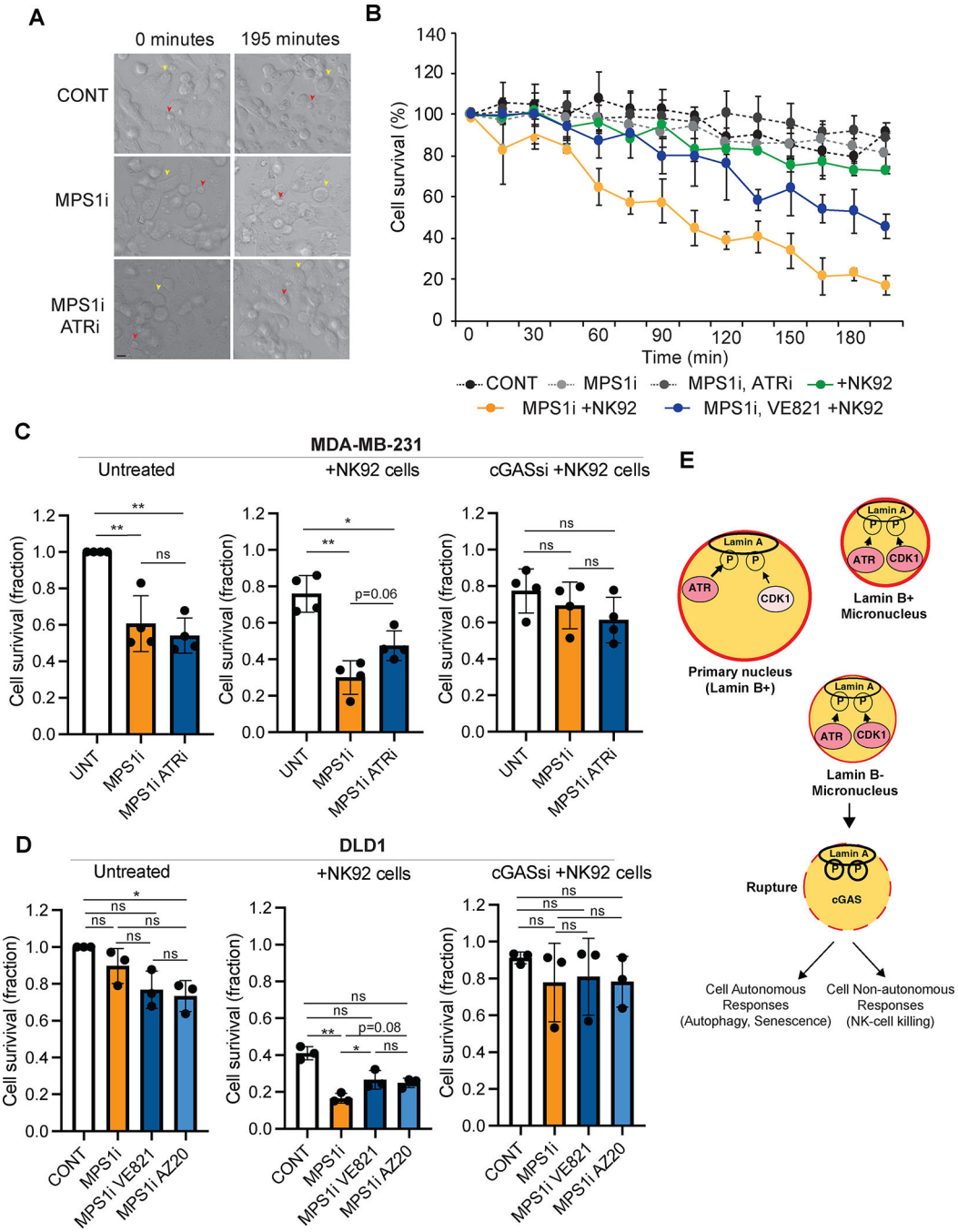

Figure 6. ATR promotes NK cell-mediated killing of MN-bearing cells.

(**A**) Representative bright-field images from live-cell imaging of MDA-MB-231 and NK92 cell over time. The wells containing both cell types in the presence of MPS1i or MPS1i and ATRi. MDA-MB-231 cells are indicated with yellow arrows, and NK92 cells are indicated with red arrows.

(**B**) Percentage of MDA-MB-231 cells surviving over time following addition of NK92 cells and live-cell imaging. Error bar: SEM from n=3 experiments.

(**C**) Fraction of MDA-MB-231 cells surviving under the indicated conditions. Prior to the addition of NK92 cells, MDA-MB-231 cells were treated with MPS1i or MPS1i and ATRi for 24 hours.
(**D**) Fraction of DLD1 cells surviving under the indicated conditions. Prior to the addition of NK92 cells, DLD1 cells were treated with MPS1i or MPS1i and ATRi for 24 hours.
(**E**) A model of the function of ATR in regulating MN rupture.
Error bars in all panels represent SEM. *P ≤ 0.05, **P ≤ 0.01, ANOVA with multiple comparisons with Tukey's correction was performed for panels comparing more than 2 conditions. Two-tailed *t*-test was used for panels with only two conditions. Scale bar: 10 μm.

KEY RESOURCES TABLE

REAGENT or RESOURCE	SOURCE	IDENTIFIER
Antibodies		
ACA (Anti-centromere antibody)	Antibodies Inc.	Cat#15-234-0001
ATR	Bethyl Laboratories	Cat#A300-138A
p-ATR T1989	GeneTex	Cat#GTX128145
CDK1	Invitrogen	Cat#MA5-11472
p-STING S366	Cell Signaling Technology	Cat#19781
STING	Cell Signaling Technology	Cat#13647
p-IRF-3 S396	Cell Signaling Technology	Cat#4947
IRF-3	Cell Signaling Technology	Cat#4302
LC3A	Cell Signaling STechnology	Cat#4599
p62	Cell Signaling Technology	Cat#5114
Lamin A/C	Cell Signaling Technology	Cat#4777
p-Lamin A Ser22	Cell Signaling Technology	Cat#13448
p-Lamin A S392	Invitrogen	Cat#PA5-38290
Lamin B	Cell Signaling Technology	Cat#12586
γH2AX	Cell Signaling Technology	Cat#9718
p-RPA32 S33	Bethyl	Cat#A300-246A
RPA32	Abcam	Cat#Ab2175
pS/T-Q ATR/ATM substrate antibody	Cell Signaling Technology	Cat#2851
Alexa Fluor 647 anti-Human	Jackson Immuno Research	Cat#109-605-088
Alexa Fluor 647 anti-Mouse	Jackson Immuno Research	Cat#15-605-150
Alexa Fluor 647 anti-Rabbit	Jackson Immuno Research	Cat#711-585-605- 152
Alexa Fluor 488 anti-Mouse	Jackson Immuno Research	Cat#715-545-150
Alexa Fluor 488 anti-Rabbit	Jackson Immuno Research	Cat#711-545-152
Alexa Fluor 594 anti-Mouse	Jackson Immuno Research	Cat#715-585-150
Alexa Fluor 594 anti-Rabbit	Jackson Immuno Research	Cat#711-585-152
Chemicals, peptides, and recombinant proteins		
VE-821 (ATRi)	Cayman Chemical	17587

REAGENT or RESOURCE	SOURCE	IDENTIFIER
AZ20 (ATRi)	Cayman Chemical	17589
RO-3306 (CDK1i)	Cayman Chemical	15149
MK-8776 (CHK1i)	Cayman Chemical	18131
K03861 (CDK2i)	Millipore Sigma	SML2971
Reversine (MPS1i)	Cayman Chemical	10004412
KU-55933 (ATMi)	Cayman Chemical	16336
Aphidicolin (APH)	Millipore Sigma	178273
Deposited data		
Generated imaging and Western blot data	This study	Mendeley Data: DOI: 10.17632/z685kkn249.1
Experimental models: Cell lines		
U2OS	ATCC	Cat#HTB-96
MDA-MB-231	nATCC	Cat#HTB-26
HeLa	ATCC	Cat#CCL-2
NK 92 mi	ATCC	Cat#CRL-2408
Oligonucleotides		
ATR siRNA - 5'-CCUCCGUGAUGUUGCUUGA-3'	ThermoFisher	N/A
cGAS siRNA - 5'-CGUGAAGAUUUC UGCACCU-3'	ThermoFisher	N/A
p62 siRNA - 5'-AUUGUGAACCCAGAAGGGC-3'	ThermoFisher	N/A
RPA siRNA - 5'- GCACCUUCUCAAGCCGAAA-3'	ThermoFisher	N/A
ISG56 Forward - 5'-TTGATGACGATGAAATGCCTGA-3'	ThermoFisher	N/A
ISG56 Reverse - 5'-CAGGTCACCAGACTCCTCAC-3'	ThermoFisher	N/A
ApoBec3G Forward - 5'-GCATCGTGACCAGGAGTATGA-3'	ThermoFisher	N/A
ApoBec3G Reverse - 5'-GTCAGGGTAACCTTCGGGT-3'	ThermoFisher	N/A
IL6 Forward - 5'-GGAGACTTGCCTGGTGAAAA-3'	ThermoFisher	N/A
IL6 Reverse - 5'-GTCAGGGGTGGTTATTGCAT-3'	ThermoFisher	N/A
GAPDH Forward - 5'-GACCCCTTCATTGACCTCAAC-3'	ThermoFisher	N/A
GAPDH Reverse - 5'-CTTCTCCATGGTGGTGAAGA-3'	ThermoFisher	N/A
Lamin A EcoRI Forward - 5'-AAAAAAGAATTCGATGGAGACCCCGTCCCAGCG-3'	ThermoFisher	N/A
Lamin A PacI Reverse - 5'-AAAAAATTAATTAATTACATGATGCTGCAGTTCTGG-3'	ThermoFisher	N/A
Recombinant DNA		
pQC NLS-YFP IX plasmid	Connie Cepko; Addgene	37341
pmRFP LC3 plasmid	Tamotsu Yoshimori; Addgene	21075
Lamin A WT-mCherry plasmid	This paper	N/A
Lamin A 392A-mCherry plasmid	This paper	N/A
Lamin A 392D-mCherry plasmid	This paper	N/A
Lamin A 395A-mCherry plasmid	This paper	N/A
Lamin A 395D-mCherry plasmid	This paper	N/A

REAGENT or RESOURCE	SOURCE	IDENTIFIER
Lamin A 392A 395A-mCherry plasmid	This paper	N/A
Lamin A 392D 395D-mCherry plasmid	This paper	N/A
Lamin A-GFP plasmid	John Eriksson Lab	N/A